Study and Comparison of Petrology and Petrogenesis Plio-Quaternary basaltic lavas of Kaleybar, Varzeqan- Ahar- northwestern of Iran

M.Fazelihagh[1*]; N.Amel[2]; A.Jahangiri[3]; M.Moayyed[4], H.Kawabata [5]

[1]PhD candidate of Petrology, Department of Earth Sciences, Faculty of Natural Sciences, Tabriz University, Tabriz, Iran m.fazeli@tabrizu.ac.ir; https://orcid.org/0009-0001-0713-164x
[2]PhD in petrology, Professor, Department of Earth Sciences, Faculty of Natural Sciences, Tabriz University, Tabriz, Iran n.amel@tabrizu.ac.ir; https://orcid.org/0000-0002-4051-188X
[3]PhD in petrology, Professor, Department of Earth Sciences, Faculty of Natural Sciences, Tabriz University, Tabriz, Iran a_jahangiri@tabrizu.ac.ir
[4]PhD in petrology, Professor, Department of Earth Sciences, Faculty of Natural Sciences, Tabriz University, Tabriz, Iran moayyed@tabrizu.ac.ir
[5]PhD in petrology, Professor. Department of Earth Science, Factulty of Science and Technology, Kouchi University, Japan, hiroshik@kochi-u.ac.ir

Abstract: The study areas are part of the Iran-Turkey Plateau and are located in the central part of the Arabian-Eurasian collision zone. The basaltic volcanic units studied are located in northwestern of Iran and East Azerbaijan Province and are of Plio-Quaternary age according to stratigraphic evidence. These lavas are composed of basalt, basaltic andesite, trachybasalt, basalt-trachyandesite and trachyandesite. Their main minerals include plagioclase, pyroxene, olivine, amphibole, and minor minerals include apatite, quartz, and opac minerals. In rock samples, the textures of the rocks are diverse and include microlithic porphyritic, hyaloporphyritic, porphyritic and trachytic textures. Clinopyroxenes are of the augite and diopside types and are alkaline and subalkaline in nature, and all of them are located in the igneous rocks range. The environment in which clinopyroxenes formed had high oxygen fugacity and they formed at low to moderate pressures. The amount of magmatic water at the time of clinopyroxene formation was moderate to low and these minerals formed at less than 10 kbar water barometric pressure. The mineralogical composition of plagioclase phenocrysts is andesine, bitonite, labradorite and oligoclase. The amphiboles in the study areas are of the pargasite and schermakite type. All olivines in the study areas are of the chrysolite type and the iron-titanium oxides are of the magnetite and titanomagnetite type. Thermobarometric calculations show a temperature of 1016.23-1226.07 °C and a pressure of 3-13 kbar for the pyroxene mineral, a temperature of 1176.85-1249.90 °C and a pressure of 10.15-30.86 kbar for the plagioclase mineral, a temperature of 733.37-954.87 °C and a pressure of 5.13-10.06 kbar for the amphibole mineral, and a temperature of 1261.97-1337 °C for the olivine mineral. The results of barometric calculations of pyroxene and amphibole indicate crystallization at medium pressures and equivalent to the middle-lower crust, and barometric calculations of plagioclase indicate crystallization at greater depths and equivalent to the Earth's mantle. The studied samples are enriched in K, Ba, Rb, U and Cs. Also, the enrichment in LILE elements and depletion in HREE elements indicate that these rocks originate from an asthenosphere mantle with a garnet source and low relative melting point. The reason for the presence of positive anomalies of K, Ba, Rb, U and Cs

https://doi.org/10.5281/zenodo.16876847

and negative anomalies of Ta, Nb and Ti can be interpreted in relation to crustal contamination. Based on the distribution coefficients of La and Y elements, the source rock of the studied samples contains 6 to 30% garnet. Examination of the tectonic structure of the samples has shown post-collisional volcanic arcs for these areas.

Keywords: Pyroxene, plagioclase, amphibole, olivine, geochemistry, petrology, thermobarometry, post-collisional, Plioquaternary, northwestern of Iran.

Introduction: Northwestern of Iran includes part of the Iran-Turkey Plateau, which is located in the central part of the Arabia-Eurasia collision zone. Like the rest of Iran, the crustal structure and magmatic evolution of northwestern of Iran have been influenced by the convergence of Arabia and Eurasia since the Mesozoic. This region includes the northern part of the Urmia-Dokhtar magmatic arc, which is parallel to the Zagros mountain range and forms a Neotethyan subduction magmatic arc (Bavali et al, 2016). Cenozoic igneous rocks are widely distributed in the Turkish-Iranian high plateau and in the northeastern part of the Bitlis-Zagros region (Dilek et al, 2010). The Mesozoic geology of Iran to this day is largely related to the subduction of the Tethys Ocean and the collision between Arabia and Eurasia, which began in the late Eocene-early Oligocene (Berberian and King, 1981). Subduction and subsequent collision between the Arabian and Eurasian plates resulted in the formation of magmatic arcs and the Turkic-Iranian plateau (Shengor and Kidd, 1979), which is mainly covered by Middle Miocene to Quaternary volcanic rocks.

Mantle-derived volcanic rocks with geochemical characteristics similar to oceanic island basalts (OIB) with or without subduction features are commonly found in the Turkish-Iranian high plateau (Dilek and Altunkaynak, 2009; Kheirkhah et al, 2009; Elitok et al, 2010; Allen et al, 2013).

According to studies conducted by Moayyed (Moayyed, 2002) on the Tertiary magmatism of Western Alborz-Azerbaijan, it has been determined that the Eocene volcanic rocks of Azerbaijan have a high-potassium calc-alkaline composition and shoshonite, which were formed in a post-collisional environment. Basalt volcanic units are located in the northwest of Iran and East and West Azerbaijan provinces and, according to stratigraphic evidence, have a Plio-Quaternary age (Amel, 2007). Quaternary volcanic activities in the northwest region of Iran are visible in places such as Nir, Sarab, Mianeh, Ahar, Varzeghan, Kaleybar, Mako, etc., and these activities originate from deep parts of the crust or mantle (Kheirkhah et al, 2009).

Middle Miocene to Quaternary volcanic rocks are visible in the large areas of Azerbaijan and northwestern Iran. The data analysis and results do not specify the tectonic setting associated with subduction, and also, these results confirm the tectonic setting associated with post-collisional arcs, which are related to processes such as delamination of a piece of the underlying crust (Lechmann et al, 2018). Several drivers for melting in northwestern Iran and its surrounding areas have been proposed, including: resubduction of the Arabian plate beneath eastern Anatolia (Rotstien and Kafka, 1982), detachment and northward movement of the subduction plate beneath eastern Anatolia (Innocenti et al, 1981), genesis in Late Miocene-Pliocene basins trending east-west and possibly associated with normal asthenosphere melting

 https://doi.org/10.5281/zenodo.16876847

(Tokel, 1985), Continental collision and crustal-lithospheric thickening in Anatolia (Dewey et al, 1986), regional extension in strike-slip fault systems (Pearce et al, 1990; Keskin, 2005), hotspot activity in relation to the presence of mantle plumes (Pearce et al, 1990; Keskin et al, 1998), Lower crustal buoyancy and its separation by isostasy as a response to load reduction and sedimentation in surrounding areas (Mitchel et al, 1999), lithosphere delamination (Pearce et al, 1990), slab fracture (Keskin, 2003), and small-scale sublithospheric convection (Kaislaniemi et al, 2014).

The Arabian-Eurasian collision zone is a result of Turkic-type orogeny (Shengor et al, 2008), characterized by subduction, accretion, and collision processes of a number of microcontinents. The microcontinents that broke away from Gondwana began to rise in a banded manner along the margins of Eurasia or Arabia since the Jurassic (Stampfli and Borel, 2002). As caducous basement rocks are visible in the region (Figure 1), the best examples being the Bitlis-Puturge massif, the Tauride massif and the Sanandaj-Sirjan belt, which are estimated to be between 600 and 540 million years old (Ustaomer et al, 2009; Moghadam et al, 2014; Beyarslan et al, 2016). The closure of the Neotethys led to the formation of ophiolitic mélanges along the two main areas of Bitlis-Zagros in the south and Erzincan-Kars in the north. Before that, Neotethys subduction around the CIA (Caucasus-Iran-Anatolia) volcanic zone produced extensive arc magmatic rocks from the Cretaceous to the Paleogene (Lin et al, 2020).

Most researchers believe that the final collision of Arabia with Eurasia occurred between 35 and 20 million years ago (Allen and Armstrong, 2008; McQuarrie and Van Hinsbergen, 2013). The collision, or closure of the Neo-Tethys, is likely to have occurred intermittently along the Bitlis-Zagros and due to the oblique contact between the two continents (Chiu et al, 2013; McQuarrie and Van Hinsbergen, 2013), during which time extensive volcanic eruptions occurred in the region. Most studies have focused on the younger and more extensive stages of volcanism in the region, which occurred from the Pliocene to the Quaternary, so different geodynamic models account for magma production in these areas. Since the chemical composition of the minerals in the study areas has not been investigated so far, in this study we will investigate the physicochemical properties of the minerals. The aim of this study was to study the petrography, geochemistry and tectonic setting of magmatism, the chemical composition of the minerals and thermobarometry of the Quaternary rocks of Kaleybar-Ahar-Varzeghan (northwest Iran).

 https://doi.org/10.5281/zenodo.16876847

ISSN: 0369-8963

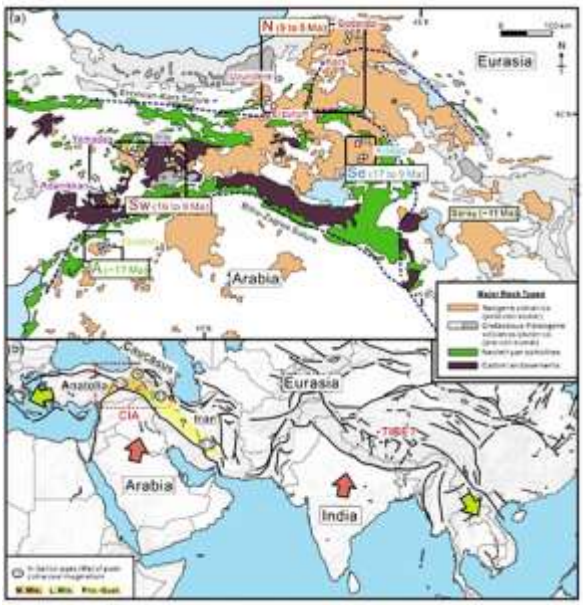

Figure 1: The Arabia-Eurasia collision zone resulting from Turkic-type orogeny (Lin et al, 2020).

Discussion:

- Geographical and geological location of the studied areas: The study areas are located at longitudes 45°46' to 15°47' East and latitudes 25°38' to 39°00' North. There is no information in the study areas due to the lack of outcrops of formations older than the Late Cretaceous, but according to what is observed in the adjacent areas, the basin in question has been uplifted as a result of the Late Cimmerian tectonic event. No traces of Early Cretaceous rocks can be seen in this area. The absence of these deposits could be related to their lack of formation. However, the presence of basal conglomerates related to Late Cretaceous deposits can be considered evidence of a tectonic phase that is likely related to the Austrin events, and this could also be a consequence of the Late Cimmerian folding. The forces that caused these events to occur were mostly compressive, the result of which could be an expansion phase that caused cracks in the Earth's crust and caused lava to come out of these cracks. The environment of formation of such rocks is often submarine and of pyroclastic type. The lavas mostly have a composition of trachyandesitic or latitic, basaltic andesite and olivine alkaline basalt. Shallow to continental sedimentary basins dominated the region in the Oligocene-Miocene and were folded as a result of the final Alpine phase, emerging from the water and creating anticlines and rifts in the south of the region. The last stage of sedimentation in the region is related to the Pliocene period, and the sediments of this time also mostly indicate lacustrine environments, whose thickness reaches about 100 meters. Finally, volcanic eruptions occurred due to the volcanic phases of the Quaternary period, causing abundant basaltic material to be ejected. The studied areas are shown in the 1:250,000 Ahar map in Figure 2 and in the 1:100,000 Varzeghan and Kaleybar map in Figure 3.

 https://doi.org/10.5281/zenodo.16876847

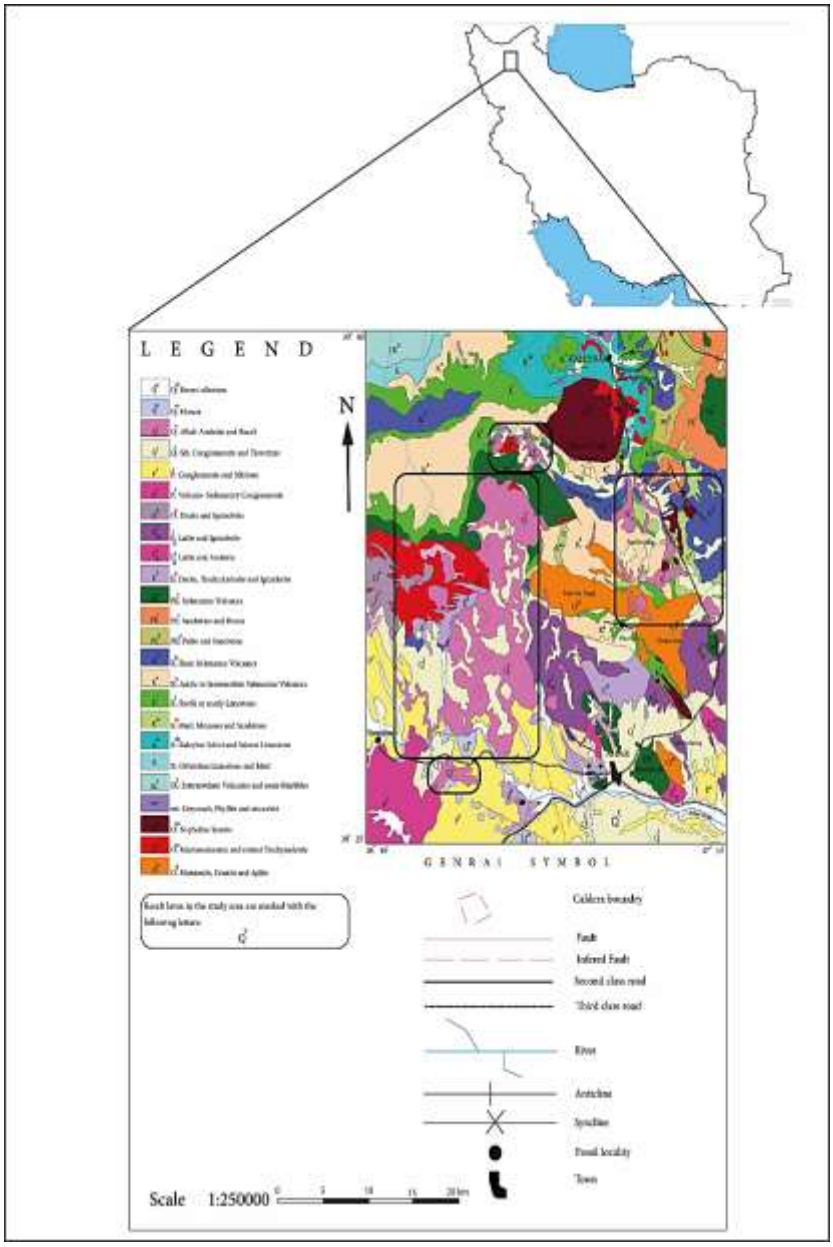

Figure 2: Study areas on the 1:250,000 Ahar geological map

https://doi.org/10.5281/zenodo.16876847

ISSN: 0369-8963

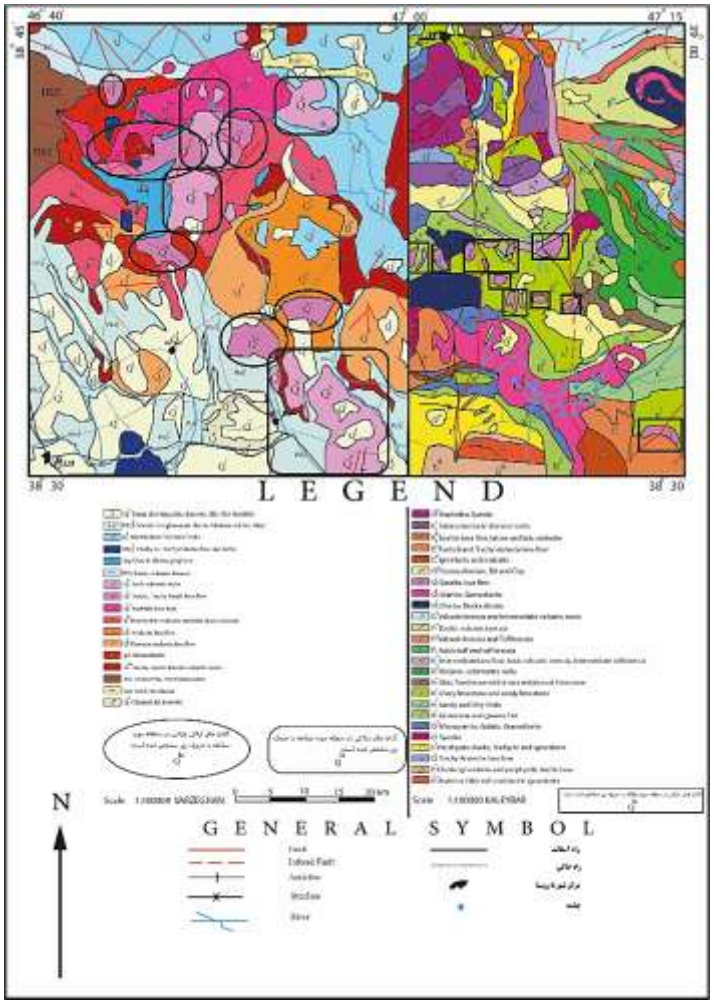

Figure 3: Study areas in 1:100,000 geological maps of Varzaghan and Kalibar

The outcrop of young basic lavas in the Kaleyber area has created extensive basaltic prisms, and their thickness may reach more than 50 meters. In the study area, these lavas are recognizable and visible with a dark color and a composition of basalt and basaltic andesite. In most outcrops, the lavas are overlain by alluvial deposits or Eocene volcanic and sedimentary units (Fig. 4, a, b, c). Quaternary volcanic lavas in the Ahar-Varzeghan region are diverse and widely distributed, and on the Ahar-Varzeghan route, volcanic products in the form of pyroclastic units such as agglomerates, tuffs, and shear lavas can be seen alternating with sedimentary units and epiclasts. Young basic lavas of Quaternary age are located around the road with a dark gray color on top of Pliocene gangue and siltstone deposits. In the villages of Gangalabad and Laleh Bejan, the aforementioned lavas have a prismatic structure and their thickness reaches more than 50 meters and include basaltic andesite, trachybasalt, basaltic trachyandesite, and trachyandesite. Volcanic activity in this region was not centralized, but eruptions occurred mainly through fractures or weak zones in a scattered manner with numerous lava flows and volcanic materials (Figure 4, d, e, f).

https://doi.org/10.5281/zenodo.16876847

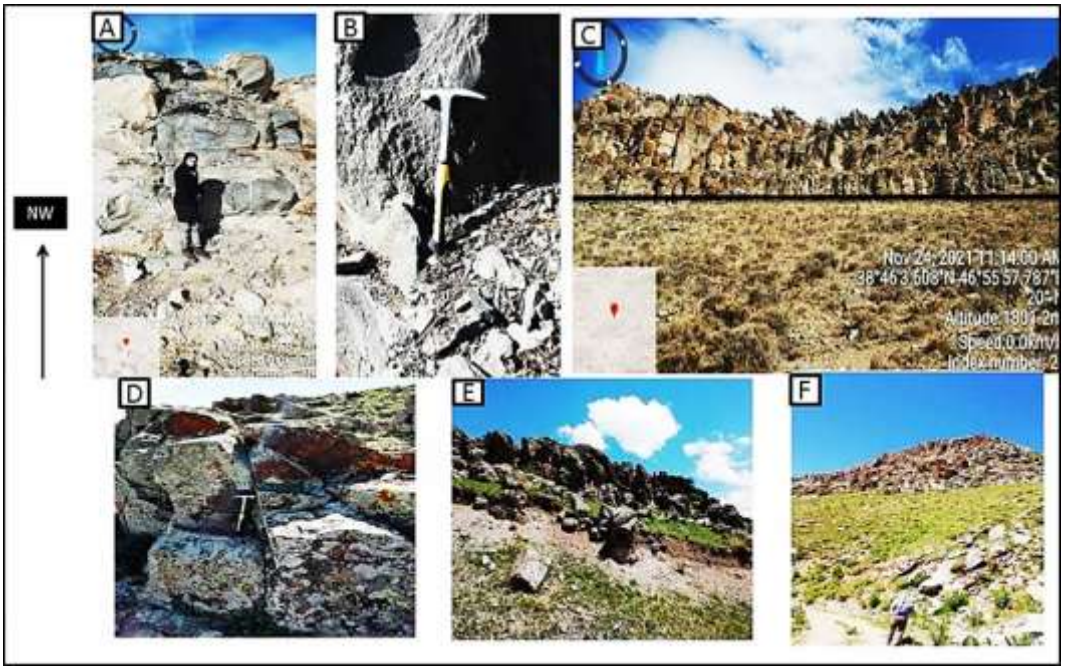

Figure 4: Outcrops of the studied rocks in the Kaleybar, Ahar, and Varzeghan regions.

- Petrography: The basaltic and basaltic andesite and trachybasalt rock samples of the Kaleybar, Ahar and Varzeghan regions are the youngest volcanic units and have a Quaternary age. The rock samples studied in hand samples are light gray in color and the rocks include microlithic porphyric, hyaloporphyric, and porphyric textures in microscopic sections. Olivine basalt rocks contain smaller amounts of olivine in the form of fine crystals. The microlithic background consists mostly of fine-bladed plagioclases with simple twinning of albite, clinopyroxene, and to a lesser extent amphibole, biotite, and opaque minerals. Pyroxenes are mostly present as coarse-grained phenocrysts, with semi-circular to ellipsoidal crystals. Trachytic texture is also visible in some samples (Figure 5, A). Some samples have a glomeroporphyritic texture with accumulation of coarse pyroxene or plagioclase crystals (Figure 5, B). The formation of glomerocrysts may partly explain the sedimentation of plagioclases in the basic masses, where plagioclase crystals have a lower density than the surrounding magma. Plagioclase often exhibits disequilibrium textures in volcanic rocks, usually reflecting changing physical conditions in the magmatic system. Sieve texture is a common sieve texture of plagioclase and pyroxene minerals in volcanic rocks, with fine, regular inclusions of background minerals within the phenocrysts. Some authors interpret it as a result of magmatic mixing (Nixon and Pearce, 1987) (Fig. 5, C). The clinopyroxene-quartz corona texture can also form when a quartz zinocryst is trapped within a basaltic magma. This xenocryst is unstable in such an environment and begins to decay rapidly, releasing silicon around it and absorbing iron and magnesium in return, thus forming clinopyroxene around it. Quartz xenocrysts can be formed as a result of mixing between felsic and mafic melts, or separated from igneous rocks in the volcanic vent, or they can have a sedimentary origin (Har, 2005). Sometimes, in sections, cavities are visible that are filled with silica and calcite and surrounded by pyroxenes in the form of a fine-grained complex, and this corona texture is visible in most sections of the Kaleybar area (Fig. 5, D). The underlying textures contain

https://doi.org/10.5281/zenodo.16876847

alkaline feldspar microliths, known as trachytic textures, and may show distinct swirling around phenocrysts, indicating a source of laminar flow of crystal-rich magma (Fig. 5, E). Veins are fractures filled with oriented crystalline fibers or deposits of unoriented minerals (usually quartz, calcite, or carbonates). Veins can occur in a variety of rocks of varying thickness. Vein development is associated with the circulation of fluids in the rock, both for material transport and for propagation and vein opening. The role of fluids in the formation and growth of veins is relatively complex, and fluid pressure may fluctuate in cycles of increasing pressure, leading to fracture and opening of the vein and subsequent pressure reduction due to drainage, during which mineral precipitation occurs. Material deposited in veins may be transported from outside the system into the fractures, a process called advection, which may cause changes in the chemical and isotopic composition of a vein and its wall rock. Material deposited in veins can also be derived from the surrounding wall rock in a closed system, for example, by dissolution and precipitation of quartz or calcite, in which case the material is transported in a circulating fluid or in a stationary fluid by diffusion (Philpotts and Ague, 2009; Bons et al, 2012) (Fig. 5, F).

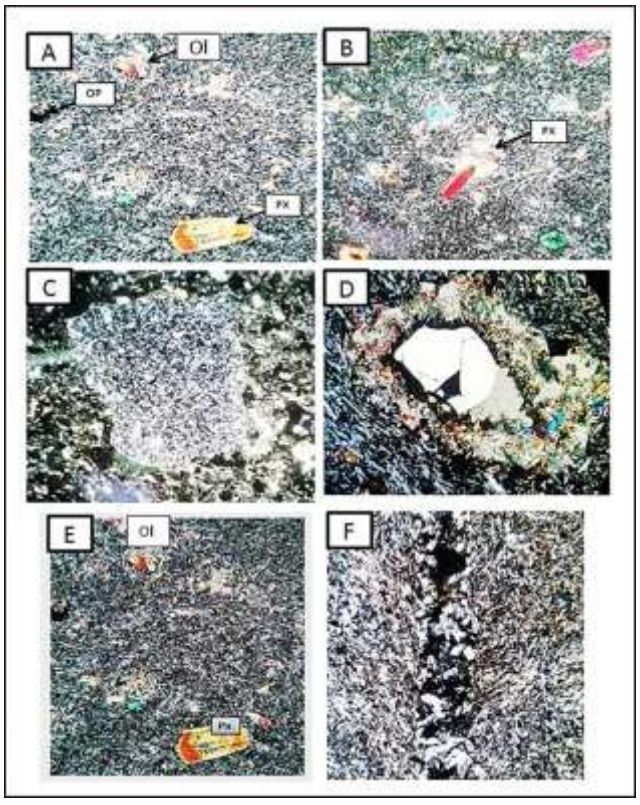

Figure 5: A) 0.625 mm scale, trachytic texture with pyroxene phenocryst and microlithic context, in XPL light
B) 0.625 mm scale, glomeroporphyritic texture with accumulation of large pyroxene crystals, in XPL light
C) 0.625 mm scale, social inclusion phenocrysts of tiny plagioclase crystals, in XPL light
D) 0.625mm scale, silica-filled voids surrounded by pyroxene crystals, in XPL light.
E) 0.625 mm scale, background textures with alkaline feldspar microlites that show swirling texture around phenocrysts, in XPL light.
F) 0.625 mm scale, veins containing quartz and plagioclase, in XPL light

Basaltic andesitic, trachyandesitic, and basaltic trachyandesitic lavas occur as scattered

 https://doi.org/10.5281/zenodo.16876847

ISSN: 0369-8963

masses in the study areas, which are gray in color in the hand sample. The main minerals include large crystals of amphibole and plagioclase with oscillatory zoning that are semi-circular and have a sieve texture, which is often caused by reduced pressure in the center and edges of the crystal and is considered a non-equilibrium texture, which are located in a fine-grained context. The texture of the rocks is porphyry with fine-grained crystals (Fig. 6, A, B). Oscillatory zoning and crystal zoning are textures that develop in solid solution minerals that are characterized optically by a change in color or extinction angle of the mineral from core to edge. This optical zoning is a reflection of chemical zoning in the mineral. Zoning is a reflection of incomplete continuum reaction relationships between the melt and the crystallized solid solution (Vernon and Clarke, 2008). In andesitic rocks, amphiboles often have burnt edges. Reaction edges are a common structure of hydrated minerals in volcanic rocks such as biotite or amphibole. Amphiboles decompose during magma ascent in response to reduced water pressure in the melt, and reaction edges on amphiboles are usually composed of a complex assemblage of minerals such as clinopyroxene, plagioclase, magnetite, and ilmenite. Amphiboles or biotite crystals release their structurally bound water into the magma in response to the reduction in water pressure in the magma as it rises to the surface (Vernon and Clarke, 2008) (Figure 6, C), and in some sections plagioclases have reactive margins (Figure 6, D). In most plagioclases, a poikilitic texture is visible, with blades of amphibole, pyroxene, and possibly zircon (Figure 6, E). Poikilitic texture refers to crystals (usually phenocrysts) in an igneous rock that contain small grains of other minerals. In igneous rocks, poikilitic texture is widely used to determine the order of crystallization of minerals. If a mineral is enclosed by another mineral, the enclosed grain should be the first to crystallize, which may sometimes be true, but certainly not always. This texture is likely the result of different nucleation and growth rates, such that one crystal (such as pyroxene) grows to a large size (low nucleation rate) in contrast to several other minerals (such as feldspars) which, with a higher nucleation rate, necessarily remain relatively small and are successively trapped in the pyroxene (McBirney, 2007).

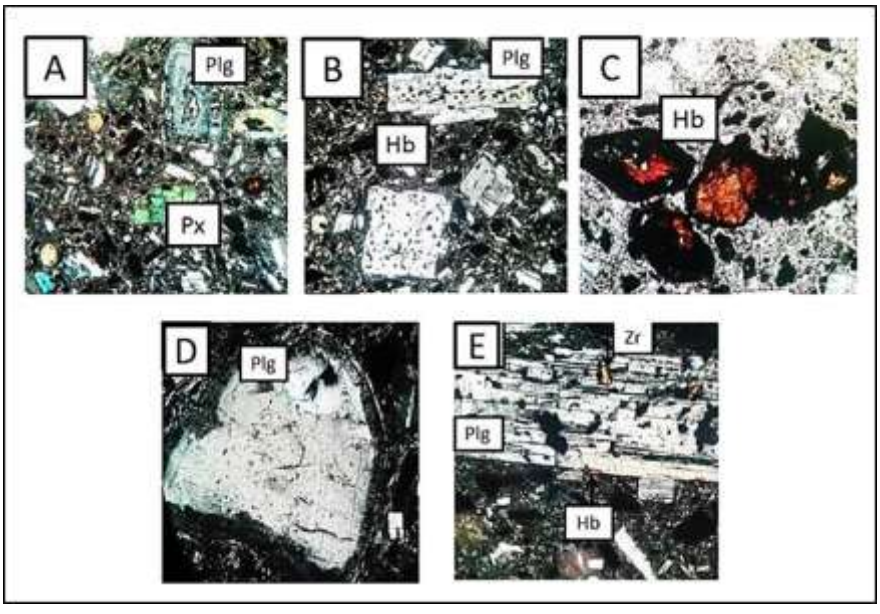

Figure 6: All sections have a scale of 0.625 mm. A) Coarse plagioclase crystals with zoned texture in XPL light

 https://doi.org/10.5281/zenodo.16876847

B) Coarse crystals of plagioclase with sieve texture, in XPL light
C) Coarse crystals of amphibole with burnt rim, in XPL light
D) Plagioclase macrocrystal with reactive rim in XPL light
E) coarse plagioclase crystal with amphibole, pyroxene and zircon blades, in XPL light

- Research Method: Field sampling was carried out in different areas of Ahar, Kaleybar and Varzeghan cities from 20 stations, and about 50 rock samples were collected. In the first stage of laboratory studies, about 40 thin sections were prepared in the rock cutting workshop of the Geology Department of Tabriz University, and then the studies of these sections were carried out in the petrology laboratory of the Geology Department. 21 samples were sent to the ZarAzma laboratory for XRF analysis and 19 samples were sent to the ICP-Ms analysis. In the XRF method, the sample is melted using lithium metaborate. The melted product is dissolved using dilute nitric acid and then the final solution is read using ICP-OES and the concentration of the main oxides is determined. The accuracy of the measuring instruments is 0.01 wt%. In the ICP-Ms method, about 100 mg of powdered samples are dissolved in Teflon glass containers with hydrofluoric acid and nitric acid, and the dry residue is dissolved in nitric acid and then in chloric acid. Some of the solution is diluted in nitric acid. The measurement accuracy is 0.01 PPM for all elements. About 20 sections were sent to Kuchi University, Japan for qualitative analysis by EDS with a microprobe (JEOL JSM-7001FA) equipped with an X-ray detector. The analytical conditions included an accelerating voltage of 15 kW, a current of 15 nanoamperes, and a counting time of 100 seconds at a working distance of 10 mm. The raw signals were matrix corrected using the ZAF correction method and calibrated against natural mineralogical standards. The relative standard deviation (RSD) of oxides is positively correlated with the abundance of mineralogical oxides, and oxides greater than 0.5 and 1.0 wt% can be analyzed with an RSD of less than 10% and 5%, respectively.

- Mineral chemistry:

- Pyroxene mineral chemistry: In the petrology of igneous rocks, pyroxene group minerals are of great importance because their compositions provide information about the state and location of crystallization. Although the pyroxene group crystallizes in two different systems, orthorhombic and monoclinic, they are related in terms of crystallographic and physical properties, as well as chemical compositions (Frost and Frost, 2014). The chemical composition formula of pyroxenes is $M_2M_1T_2O_6$, which includes one tetrahedral site (T) and two octahedral sites (M_1 and M_2). The sum of cations located in tetrahedral (T) and octahedral (M_1) positions will be 2 and 1, respectively. Cations with tetrahedral coordination, including Si4+, Al3+ and Fe3+, are located in tetrahedral position T and the remainder of cations in tetrahedral position T, Al3+ and Fe3+, are located in octahedral position M1, which consists of cations with regular octahedral coordination, but if there are not enough Al3+ and Fe3+ cations to fill the M1 position, cations such as Ti^{4+}, Zr^{4+}, Cr^{3+}, V^{3+}, Ti^{3+}, Sc^{3+}, Zn^{2+}, Mg^{2+}, Fe^{2+} and Mn^{2+} can be located in this position. The remaining cations from the M1 site (Mg^{2+}, Fe^{2+} and Mn^{2+}) are replaced by cations such as Li^{+}, Ca^{2+} and Na^{+} in the M2 octahedral site, which contains cations with a complex octahedral arrangement, which have a valence of about 1 (Morimoto et al, 1988). Pyroxenes are classified and divided by the cations present in the M octahedral site (M_1 and M_2) and based on the 6 oxygen atoms. About 373 point analyses have

 https://doi.org/10.5281/zenodo.16876847

been carried out of the pyroxenes of the region, some of which are given in Table 1.

Table 1: Chemistry results of a number of pyroxenes in the studied areas

	BZ	BZ	NB	NB	GB	GB	PBM	PBM	SB	SB	KB	KB
SiO_2	51.84	51.70	51.07	52.91	48.38	46.51	50.44	50.62	52.02	52.20	52.16	50.80
TiO_2	0.24	0.55	0.68	0.40	1.81	2.69	0.96	1.08	0.43	0.44	0.77	1.05
Al_2O_3	1.28	2.39	4.12	2.28	5.12	6.34	3.70	4.48	1.97	1.66	3.04	3.28
FeO	9.23	6.08	5.22	4.89	7.46	7.31	6.84	6.82	10.07	9.74	6.32	7.27
MnO	0.69	0.08	0.16	0.06	0.03	0.15	0.10	0.08	0.44	0.42	0.16	0.16
MgO	13.64	15.76	15.93	17.20	13.70	12.90	14.62	14.70	14.58	14.78	15.66	15.17
CaO	21.91	22.68	21.78	21.73	23.48	22.89	22.68	22.23	20.94	20.99	22.27	22.40
Na_2O	0.60	0.38	0.02	0.00	0.38	0.82	0.56	0.68	0.33	0.34	0.57	0.44
Total	99.43	99.69	99.61	99.97	100.41	99.73	99.98	100.74	100.81	100.58	100.06	100.64
Si	1.956	1.917	1.884	1.936	2.407	2.338	1.875	1.863	1.933	1.941	1.907	1.878
Ti	0.007	0.015	0.019	0.011	0.068	0.102	0.027	0.030	0.012	0.012	0.021	0.020
Al	0.570	0.104	0.179	0.099	0.300	0.376	0.162	0.194	0.086	0.073	0.131	0.143
Fe	0.291	0.188	0.161	0.149	0.310	0.307	0.213	0.210	0.313	0.303	0.193	0.225
Mn	0.022	0.003	0.005	0.002	0.001	0.007	0.003	0.003	0.014	0.013	0.005	0.005
Mg	0.767	0.871	0.876	0.938	1.016	0.967	0.810	0.807	0.807	0.819	0.853	0.836
Ca	0.886	0.901	0.861	0.852	1.252	1.232	0.903	0.877	0.834	0.836	0.872	0.887
Na	0.044	0.027	0.044	0.032	0.036	0.080	0.040	0.049	0.024	0.024	0.040	0.031
Total	4.031	4.028	4.029	4.019	5.392	5.411	4.036	4.033	4.023	4.022	4.024	4.036
#Mg	72.48	82.21	84.47	86.25	76.61	75.87	79.20	79.34	72.07	73.01	81.53	78.80
Fe^{2+}	0.199	0.102	0.072	0.090	0.098	0.053	0.103	0.109	0.241	0.234	0.116	0.113
Fe^{3+}	0.090	0.085	0.088	0.059	0.132	0.174	0.108	0.099	0.070	0.067	0.076	0.110
$Al^{(IV)}$	0.044	0.082	0.116	0.064	0.194	0.246	0.125	0.136	0.067	0.059	0.092	0.121
$Al^{(VI)}$	0.013	0.022	0.063	0.035	0.031	0.036	0.037	0.058	0.019	0.014	0.039	0.022
Wo	44.11	45.29	44.25	43.18	47.90	47.62	45.90	45.12	41.89	41.93	44.43	44.75
En	38.21	43.80	45.04	47.56	38.90	37.35	41.17	41.52	40.59	41.08	43.48	42.17
Fs	15.49	9.54	8.47	7.64	11.80	11.94	10.87	10.85	16.33	15.76	10.03	11.49
Ac	2.19	1.37	2.24	1.62	1.40	3.09	2.05	2.51	1.19	1.23	2.06	1.59

 https://doi.org/10.5281/zenodo.16876847

ISSN: 0369-8963

To determine the type of pyroxene, the En, Wo, Fs diagram can be used (Morimoto et al, 1988). Accordingly, the composition of clinopyroxenes in the above areas is in the diopside and augite range (Figure 7). Clinopyroxenes are petrogenic minerals that are more resistant to alteration and their composition can be used to determine the type of magmatic series in them (Letterrier et al, 1982). The amounts of Si, Al and Ti within the pyroxene structural network depend on the degree of alkalinity and using this characteristic, magmatic series can be distinguished. Using the amounts of SiO2 and Al2O3 in the chemical composition of pyroxenes, peralkaline, alkaline and subalkaline magmatic series can be distinguished (LeBase, 1962) (Figure 8). In this diagram, the clinopyroxenes of the Zandabad region are mostly in the subalkaline range and a smaller number of them are in the alkaline range, the clinopyroxenes of the Siahkalan region are in the subalkaline range, the clinopyroxenes of the Kaleybar, Gangalabad, Marzroud and Nahar regions are in the subalkaline and alkaline ranges.

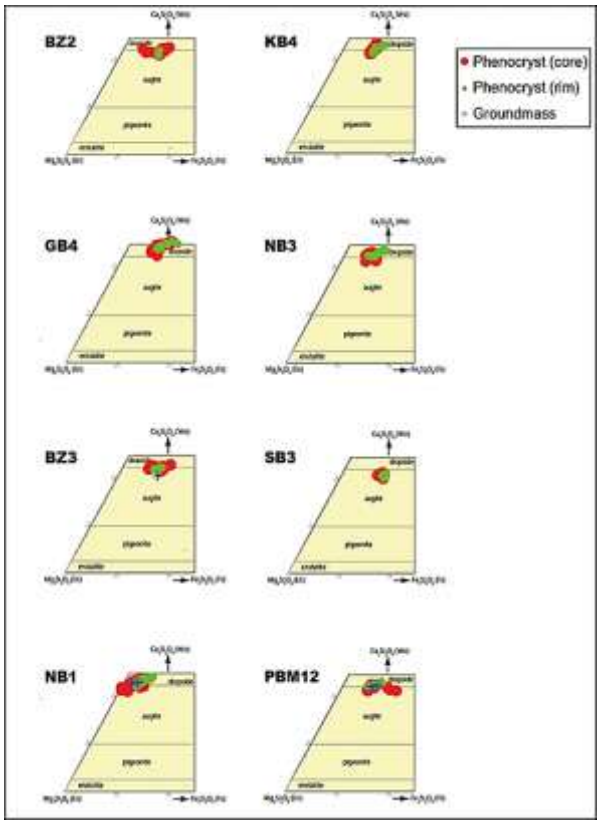

Figure 7: Representation of the composition of pyroxenes in the ternary system Wo, En, Fs (Morimoto et al., 1988).

https://doi.org/10.5281/zenodo.16876847

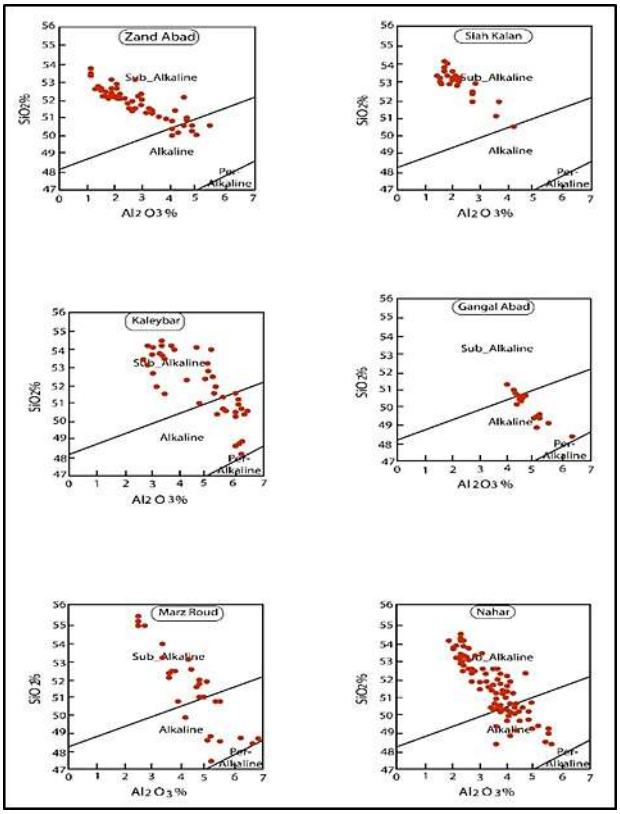

Figure 8: Ti/Ca+Na variation diagram (Leterrier et al., 1982)

Oxygen fugacity has a significant effect on the change in liquidus temperature and melt-crystal composition (France et al, 2010) and is considered one of the effective factors in controlling magmatic processes (Botcharmikov et al, 2005; Kress and Carmichart, 1991; Moretti, 2005; Ottonolle et al, 2001), and also affects the crystallization sequence and the type of crystallized minerals. The oxygen fugacity can be obtained using the Al(IV) + 2Ti + Cr versus Al(VI) + Na sum diagram, which is a function of the amount of trivalent iron in pyroxenes (Schweitzer et al, 1979). This diagram is based on Al in the tetrahedral position and Na with Al and Cr^{3+} and Ti in the octahedral position. Considering the location of the samples in this diagram, it can be said that the oxygen fugacity was high in the environment where these rocks formed (Figure 9).

https://doi.org/10.5281/zenodo.16876847

ISSN: 0369-8963

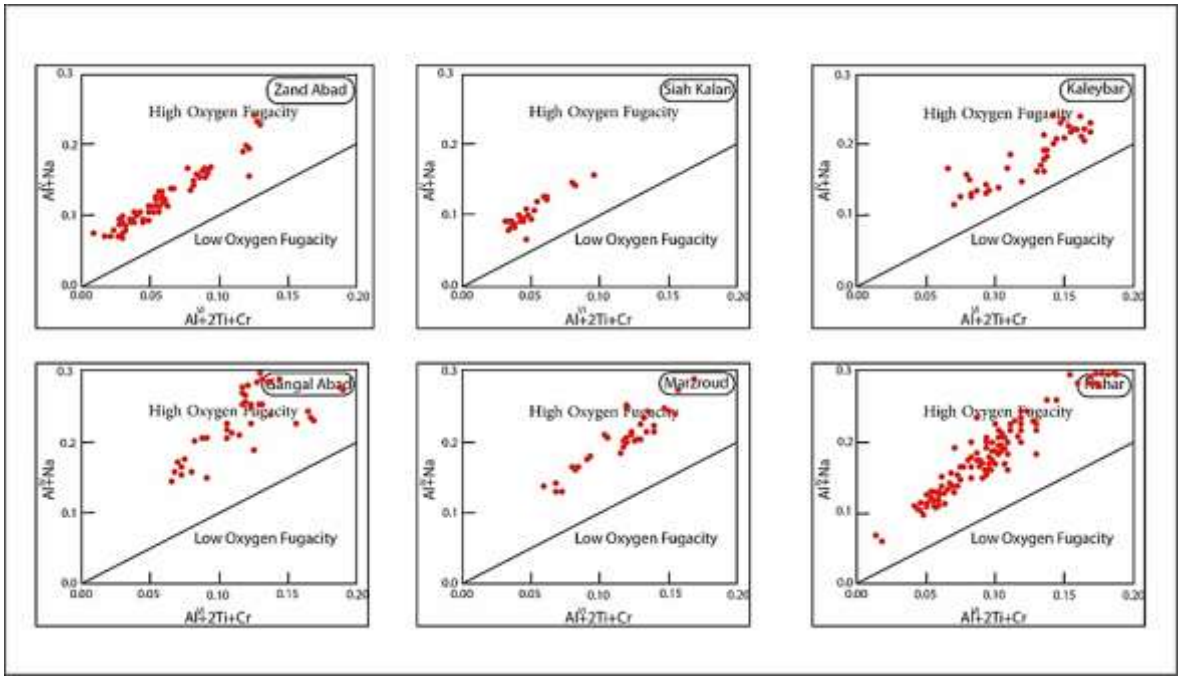

Figure 9: 2Ti+Cr+AlVI/AlIV+Na variation diagram for determining oxygen fugacity (Schweitzer et al., 1979).

The location of Al in the tetrahedral and octahedral positions of clinopyroxenes depends on the pressure and amount of water in their crystallization environment, such that the higher the amount of Al^{VI} in clinopyroxenes, the higher the pressure this mineral is formed, and the amount of Al^{IV} decreases with increasing amount of water in the crystallization environment of pyroxenes. Accordingly, according to the Al^{IV} vs. Al^{VI} diagram, the clinopyroxenes of the studied areas were formed at low to medium pressures (Figure 10) (Aoki and Shiba, 1973).

https://doi.org/10.5281/zenodo.16876847

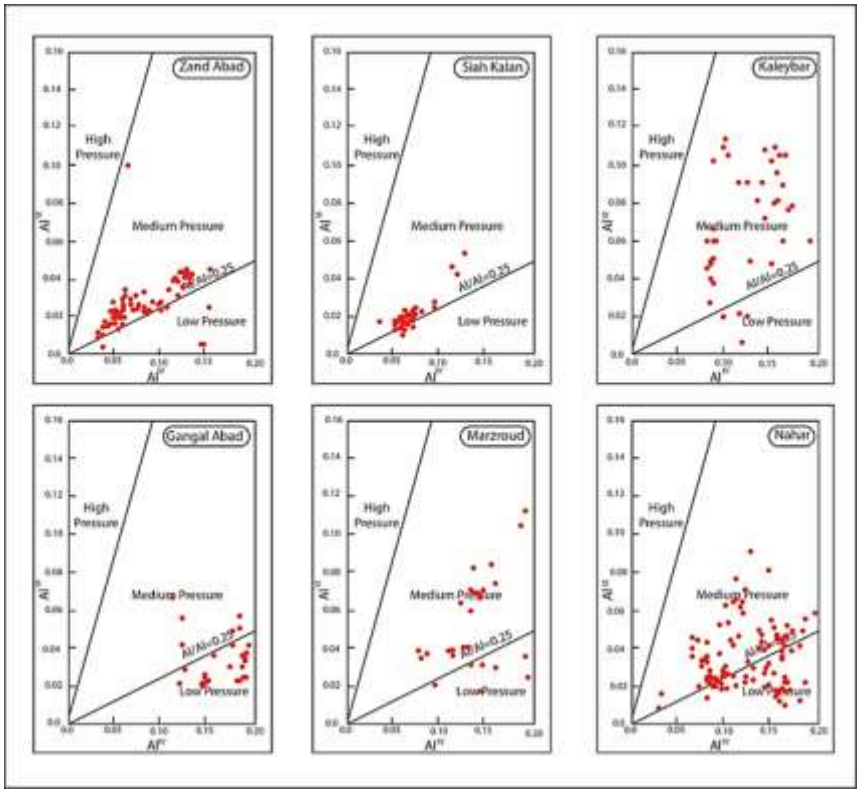

Figure 10: Based on the Al^{IV} vs. Al^{VI} diagram, clinopyroxenes in the study areas crystallized at low to moderate pressures (Aoki and Shiba, 1973)

Based on the Al^{IV} vs. Al^{VI} diagram, an approximate estimate of the percentage of magma water during mineral crystallization has been provided (Helz, 1973). According to this diagram, the amount of magma water at the time of formation of clinopyroxenes in the studied areas was medium to low, and these minerals formed in a range of less than 10 kbar of water pressure (Figure 11).

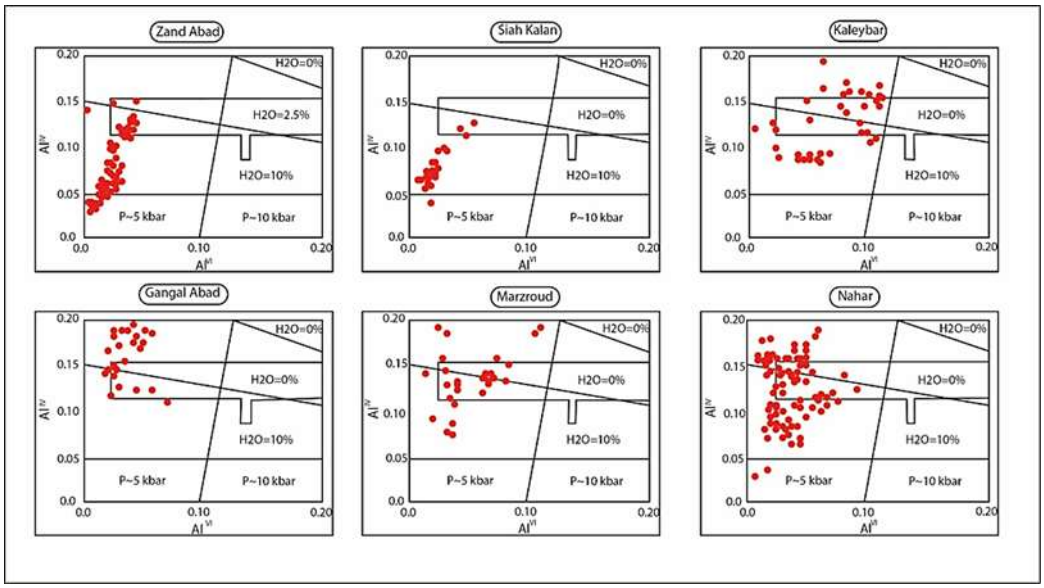

Figure 11: Location of clinopyroxenes in the studied areas in the Al^{IV} versus Al^{VI} diagram (Helz, 1973)

The value of #Mg = 100Mg/(Mg+Fe2+) for the studied clinopyroxenes has been calculated

https://doi.org/10.5281/zenodo.16876847

in the range of 64.81-90.94, which some scientists (Deer et al, 1987) believe that clinopyroxenes with high #Mg (#Mg>70) crystallized from a primary magma.

- Plagioclase Mineral Chemistry: Plagioclases are among the most abundant minerals in the studied samples, occurring both as phenocrysts and microlites. The general formula of plagioclases is (Na, Ca)(Si, Al)$_4$O$_8$. Approximately 382 point analyses of plagioclases from the Zandabad, Nahar, Gangalabad, Marzroud, Siahkalan, Lalehbejan, and Kaleybar regions were performed after calculation based on the structural formula of 8 oxygens, some of which are given in Table 2.

Table 2: Chemistry analyses of plagioclases in the study areas

	BZ	BZ	NB	GB	GB	PBM	SB	SB	LB	LB	KB	KB
SiO_2	56.31	57.26	56.91	54.97	56.42	58.69	53.60	65.48	57.89	56.63	55.59	56.75
TiO_2	0.04	0.04	0.18	0.28	0.17	0.66	0.07	0.00	0.00	0.06	0.08	0.04
Al_2O_3	26.68	25.61	27.24	26.61	26.80	25.37	28.06	21.69	26.27	26.87	28.91	27.72
FeO	0.28	0.44	1.20	0.91	0.81	1.24	1.80	0.11	0.24	0.36	0.56	0.39
MnO	0.06	0.00	0.03	0.23	0.00	0.00	0.01	0.00	0.02	0.04	0.00	0.00
MgO	0.00	0.00	0.00	0.09	0.01	0.02	0.37	0.00	0.00	0.01	0.05	0.00
CaO	9.13	8.11	9.69	9.05	8.78	7.35	11.21	2.48	8.30	9.09	11.01	9.67
Na_2O	5.97	6.42	6.21	5.75	6.22	6.01	4.79	10.24	6.56	6.12	5.39	6.19
K_2O	0.54	0.66	0.32	0.72	0.41	0.64	0.29	0.03	0.46	0.39	0.24	0.23
P_2O_5	0.17	0.22	0.11	0.42	0.19	0.18	0.12	0.23	0.16	0.16	0.14	0.18
Total	99.18	98.77	101.90	99.03	99.81	100.17	100.32	100.27	99.90	99.73	101.97	101.18
Si	2.556	2.606	2.529	2.518	2.549	7.558	2.437	2.874	2.599	2.555	2.467	2.528
Ti	0.001	0.001	0.006	0.009	0.006	0.064	0.002	0.000	0.000	0.002	0.003	0.001
Al	1.428	1.374	1.427	1.437	1.427	3.850	1.504	1.122	1.390	1.429	1.512	1.455
Fe	0.010	0.017	0.045	0.035	0.030	0.134	0.068	0.004	0.009	0.013	0.021	0.014
Mn	0.002	0.000	0.001	0.009	0.00	0.000	0.000	0.000	0.001	0.002	0.000	0.000
Mg	0.000	0.000	0.000	0.006	0.001	0.004	0.025	0.000	0.000	0.001	0.003	0.000
Ca	0.444	0.395	0.461	0.444	0.425	1.015	0.546	0.117	0.399	0.439	0.523	0.461
Na	0.525	0.566	0.535	0.511	0.545	1.500	0.423	0.872	0.571	0.535	0.463	0.535
K	0.031	0.038	0.018	0.042	0.024	0.106	0.017	0.002	0.026	0.022	0.014	0.013
Total	5.002	5.002	5.025	5.019	5.010	14.241	5.025	4.995	4.999	5.002	5.009	5.012
Ab	52.57	56.63	52.74	51.23	54.84	57.28	42.86	88.05	57.30	53.69	46.34	52.97

 https://doi.org/10.5281/zenodo.16876847

An	44.30	39.53	45.47	44.55	42.78	38.71	55.43	11.78	40.06	44.06	52.31	45.73
Or	3.12	3.83	1.79	4.22	2.38	4.01	1.71	0.17	2.64	2.25	1.36	1.30

Based on the results and graphs drawn (Deer et al, 1991), the mineralogical composition of plagioclases of the studied samples in the Zandabad, Nahar, Lalehbejan and Kaleybar areas is in the range of andesine and labradorite, in the Siahkalan area in the range of andesine and bitonite, in the Gangalabad area in the range of andesine, and in the Marzroud area in the range of andesine and oligoclase (Figure 12).

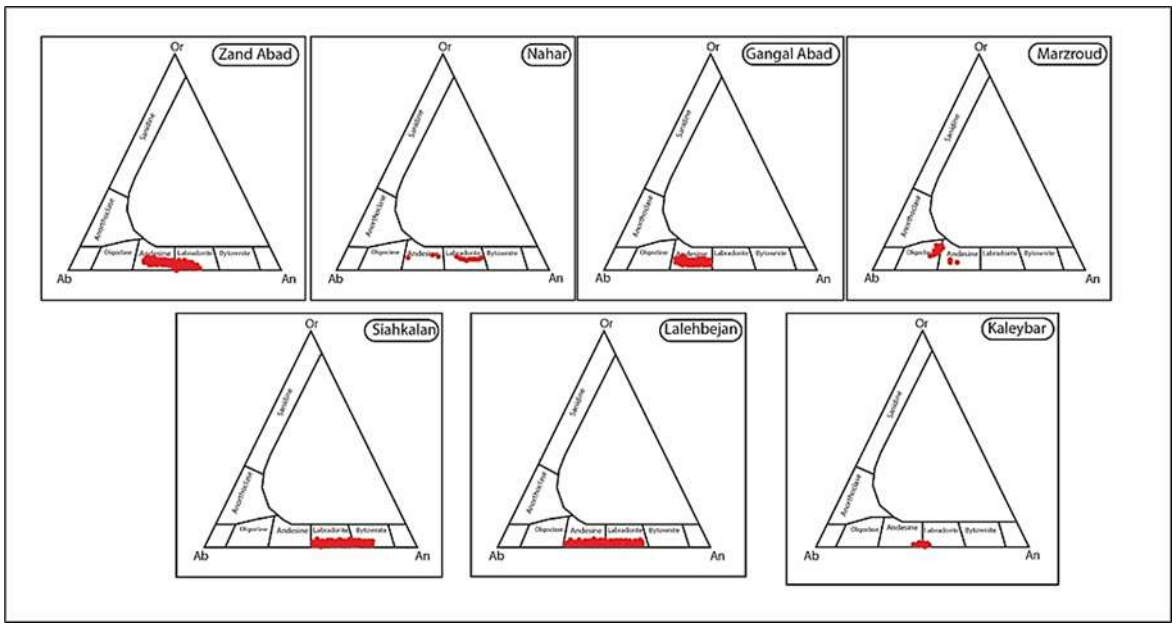

Figure 12: Plagioclase composition determination diagram (Deer et al, 1991).

Based on the ratio of plagioclase minerals and the weight percent of FeO to the mole percent of anorthite (Bown, 1928), these minerals have formed in mixed conditions that are consistent with the presence of disequilibrium textures (such as sieve textures, etc.) (Figure 13).

 https://doi.org/10.5281/zenodo.16876847

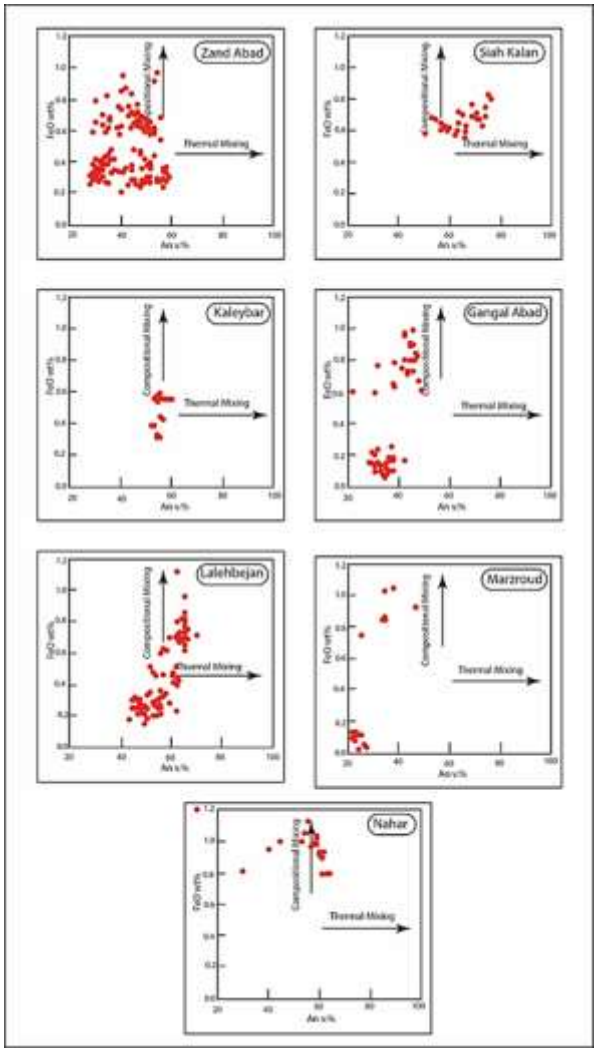

Figure 13: Mole percent anorthite versus weight percent FeO to identify inclusions in plagioclases (Bown, 1928).

Amphibole mineral chemistry: The general formula of amphibole group minerals is $A_{0-1} B_2^{VI} C_5^{IV} T_8 O_{22} (OH,F)_2$ (Deer et al, 1992; Leack et al, 1997), where A: contains large cations (Na, K), B: contains various cations (Ca, Na, Mn, Fe and Mg), C: contains medium-sized cations (Mg, Mn, Fe) and T: contains cations (Si, Al). About 130 point analyses of amphiboles from the Zandabad, Kaleybar, Marzroud and Lalehbejan areas have been carried out based on 23 oxygens, some of which are listed in Table 3.

Table 3: chemistry analyses of amphiboles in the study areas

	BZ	**BZ**	**BZ**	**KB**	**KB**	**KB**	**PBM**	**PBM**	**LB**	**LB**	**LB**
SiO_2	42.91	42.03	41.33	41.92	40.99	40.50	52.49	45.05	43.32	42.72	41.06
TiO_2	2.66	2.71	2.84	2.55	2.53	2.67	0.19	2.90	2.37	2.50	2.10
Al_2O_3	10.76	11.33	11.94	14.27	13.85	14.26	2.23	8.22	12.76	12.67	13.61
FeO	9.08	9.96	9.54	13.83	13.88	14.82	11.72	7.87	10.19	10.29	15.61
MnO	0.13	0.08	0.18	0.11	0.11	0.18	0.52	0.05	0.13	0.09	0.24

https://doi.org/10.5281/zenodo.16876847

MgO	16.04	15.03	15.57	11.90	12.26	11.40	11.43	12.89	14.99	14.80	11.16
CaO	11.76	11.90	11.67	11.94	11.85	11.81	20.18	22.33	11.72	11.80	11.40
Na_2O	2.50	2.59	2.61	2.60	2.61	2.62	2.05	0.86	2.61	2.57	2.52
K_2O	0.93	0.91	0.94	0.45	0.46	0.51	0.02	0.01	0.41	0.47	0.59
P_2O_5	0.17	0.14	0.08	0.09	0.07	0.09	0.06	0.01	0.06	0.07	0.10
Total	96.95	96.70	96.70	99.67	98.62	98.88	100.90	100.19	98.56	97.98	98.39
Si	6.316	6.238	6.129	6.102	6.049	5.995	1.966	6.492	6.260	6.224	6.117
Ti	0.295	0.303	0.316	0.279	0.281	0.297	0.005	0.314	0.257	0.274	0.235
Al	1.867	1.982	2.088	2.448	2.409	2.487	0.099	1.396	2.173	2.176	2.389
Fe	1.117	1.235	1.183	1.684	1.713	1.834	0.367	0.949	1.231	1.254	1.945
Mn	0.017	0.010	0.023	0.014	0.014	0.023	0.017	0.006	0.016	0.011	0.031
Mg	3.520	3.326	3.441	2.583	2.697	2.516	0.638	2.770	3.230	3.215	2.479
Ca	1.855	1.893	1.854	1.863	1.874	1.873	0.810	3.447	1.185	1.842	1.820
Na	0.713	0.745	0.751	0.734	0.747	0.752	0.149	0.239	0.732	0.726	0.728
K	0.174	0.172	0.178	0.083	0.086	0.096	0.001	0.002	0.075	0.087	0.112
P	0.011	0.009	0.005	0.006	0.004	0.006	0.001	0.001	0.004	0.004	0.006
Total	15.884	15.914	15.967	15.795	15.875	15.880	4.053	15.616	15.794	15.814	15.863
#Mg	75.91	72.92	74.42	60.54	61.16	57.83	63.49	74.48	72.40	71.94	56.04
Fe^{2+}	0.595	0.852	0.513	1.258	1.098	1.251	5.976	5.174	0.610	0.679	1.199
Fe^{3+}	0.511	0.376	0.654	0.412	0.594	0.562	4.433	4.005	0.606	0.566	0.717
$Al^{(IV)}$	1.747	1.805	1.955	1.948	2.026	2.075	0.378	1.396	1.819	0.820	1.974
$Al^{(VI)}$	0.101	0.159	0.103	0.479	0.353	0.384	0.000	0.000	0.326	0.650	0.381

According to the diagram presented by (Leack et al, 1997), the composition of amphiboles in the Zandabad, Kaleybar and Lalehbejan areas is in the pargasite range, and the composition of amphiboles in the Marzroud area is in the Tscheramakit range (Figure 14).

 https://doi.org/10.5281/zenodo.16876847

ISSN: 0369-8963

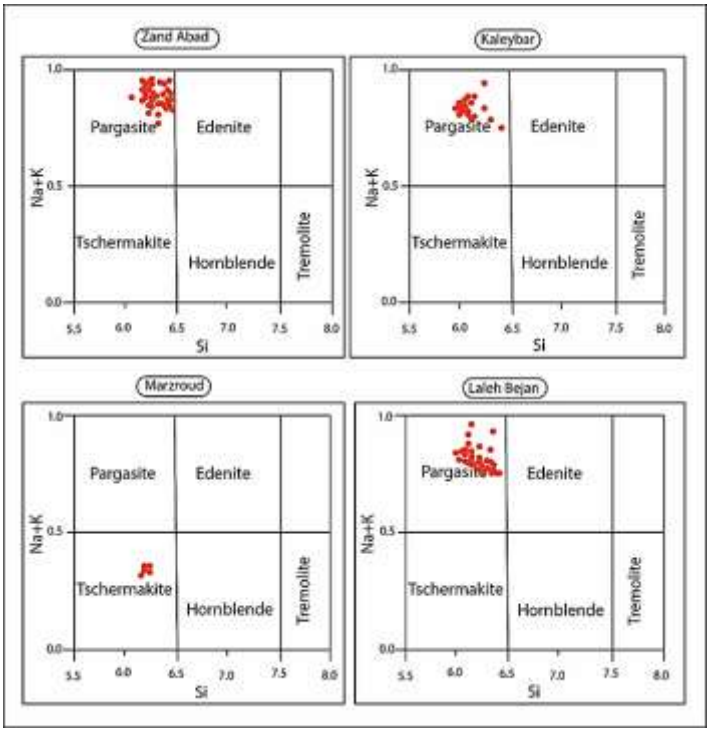

Figure 14: Diagram for determining the composition type of amphiboles (Leack et al, 1997).

Amphiboles of the subalkaline series have a lower TiO_2 content than alkaline series, and amphiboles containing 9 to 14 wt% MgO can have a TiO_2 content of about 3.5 wt%. Amphiboles of the subalkaline system also have lower Al_2O_3, K_2O, and Na_2O contents than alkaline environments (Molina et al, 2009). In the bivariate diagram of Al_2O_3 versus TiO_2, the studied amphiboles of the Zandabad and Kaleybar regions are in the alkaline-subalkaline and subalkaline ranges, the amphiboles of the Lalehbejan region are in the alkaline-subalkaline range, and the amphiboles of the Marzroud region are in the subalkaline range (Figure 15).

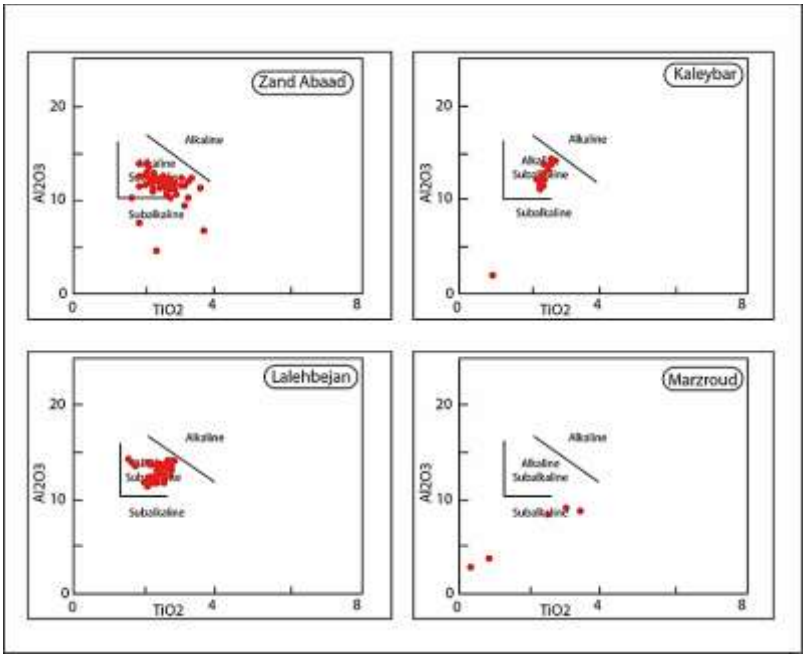

Figure 15: Determination of the magmatic series of volcanic rocks based on the chemical composition of amphiboles (Molina et al, 2009)

https://doi.org/10.5281/zenodo.16876847

ISSN: 0369-8963

Olivine mineral chemistry: The general formula of olivine is $(Mg, Fe)_2SiO_4$. The crystallographic system of olivine, which is orthorhombic, is only recognizable when olivine forms as phenocrysts in volcanic rocks (Frost and Frost, 2014). Magnesium-rich olivine melts form at higher temperatures than iron-rich olivine melts, so forsteritic olivine is typically found in the mantle or in igneous rocks that rise directly from the mantle (Frost and Frost, 2014). The type of olivine can also be determined to some extent based on the MnO percentage, with fayalite olivines containing several percent MnO (Frost and Frost, 2014), while the samples studied show MnO below one percent. Approximately 118 point analyses of olivines from the Nahar and Gangalabad regions have been performed based on the four oxygens, some of which are listed in Table 4.

Table 4: chemistry analyses of olivines in the study areas

	NB	NB	NB	NB	NB	NB	GB	GB	GB	GB	GB
SiO_2	41.42	40.98	41.19	40.30	40.63	41.08	41.19	41.55	41.57	40.16	40.43
TiO_2	0.00	0.00	0.06	0.00	0.01	0.01	0.01	0.01	0.05	0.04	0.04
Al_2O_3	0.06	0.07	0.08	0.11	0.08	0.06	0.06	0.08	0.04	0.10	0.08
FeO	11.85	11.67	10.25	11.92	11.85	10.59	10.56	10.58	9.62	14.52	13.05
MnO	0.40	0.35	0.55	0.30	0.23	0.46	0.38	0.38	0.52	0.36	0.61
MgO	48.73	48.37	49.42	47.44	47.65	49.48	49.13	49.69	50.32	45.37	46.72
CaO	0.18	0.12	0.20	0.13	0.14	0.26	0.12	0.18	0.17	0.20	0.23
Na_2O	0.10	0.05	0.08	0.04	0.07	0.09	0.07	0.10	0.04	0.06	0.04
K_2O	0.01	0.02	0.01	0.00	0.00	0.00	0.00	0.00	0.01	0.01	0.00
P_2O_5	0.03	0.13	0.04	0.06	0.11	0.09	0.01	0.09	0.06	0.16	0.07
Total	102.79	101.77	101.89	100.31	100.79	102.11	101.53	102.67	102.40	100.99	101.28
Si	0.997	0.996	0.994	0.995	0.998	0.991	0.998	0.996	0.995	0.997	0.995
Ti	0.000	0.000	0.001	0.000	0.000	0.000	0.000	0.000	0.001	0.001	0.001
Al	0.002	0.002	0.002	0.003	0.002	0.002	0.002	0.002	0.001	0.003	0.002
Fe	0.239	0.237	0.207	0.246	0.243	0.214	0.214	0.212	0.193	0.302	0.269
Mn	0.008	0.007	0.011	0.006	0.005	0.009	0.008	0.008	0.011	0.008	0.013
Mg	1.748	1.752	1.779	1.746	1.744	1.780	1.775	1.775	1.796	1.679	1.714
Ca	0.005	0.003	0.005	0.004	0.004	0.007	0.003	0.005	0.004	0.005	0.006
Na	0.005	0.002	0.004	0.004	0.003	0.004	0.003	0.005	0.002	0.003	0.002
K	0.000	0.001	0.000	0.002	0.000	0.000	0.000	0.000	0.0000	0.000	0.000
P	0.000	0.001	0.000	0.001	0.001	0.001	0.000	0.001	0.001	0.002	0.001

https://doi.org/10.5281/zenodo.16876847

Total	3.004	3.002	3.005	3.003	3.001	3.008	3.003	3.004	3.004	3.000	3.003
#Mg	87.99	88.08	89.58	87.64	87.76	89.28	89.24	89.33	90.31	84.77	86.46
Fo	87.639	87.763	89.075	87.373	87.548	88.863	88.893	88.986	89.839	84.459	85.451
Fa	11.953	11.876	10.362	12.314	12.212	10.668	10.717	10.627	9.633	15.161	14.167
Tp	0.409	0.361	0.563	0.314	0.240	0.469	0.391	0.387	0.527	0.381	0.381

According to the data in the tables and graphs presented (Deer et al, 1992), all olivines in the studied areas are located in the chrysolite range (Figure 16).

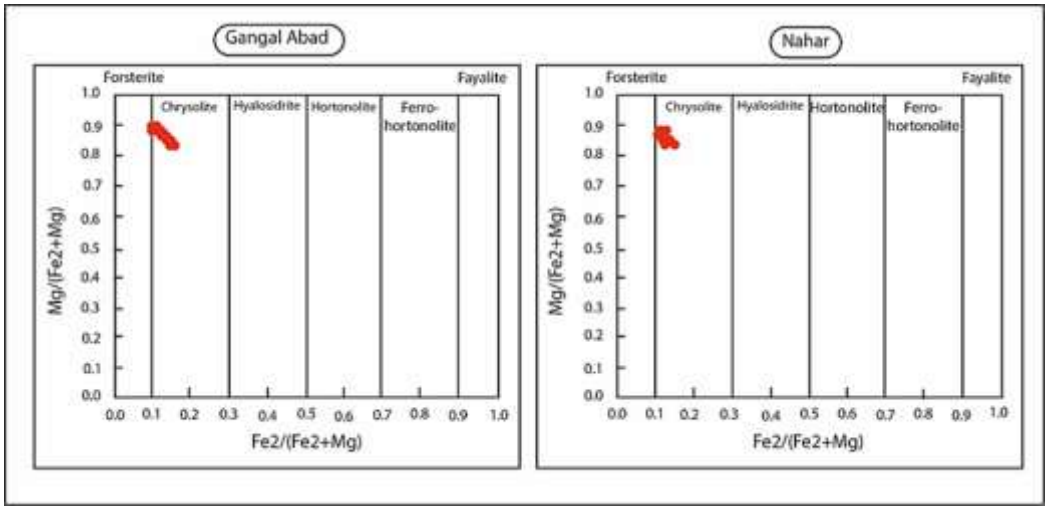

Figure 16: Diagram of olivine composition determination in the studied areas (Deer et al, 1992).

- Iron- titanium mineral chemistry: To determine their type and chemical composition, 130 spot analyses were carried out from the areas of Zandabad, Nahar, Marzroud, Gangalabad, Kaleybar, Siahkalan and Lalehbejan, some of which are given in Table 5.

Table 5: Chemistry analyses of iron-titanium oxides in the study areas

	BZ	**BZ**	**NB**	**NB**	**PBM**	**GB**	**GB**	**KB**	**KB**	**SB**	**LB**	**LB**
SiO_2	0.28	0.42	0.22	0.24	0.24	0.23	0.26	0.31	0.29	0.28	0.26	0.28
TiO_2	3.19	33.47	4.03	4.31	8.64	3.71	11.76	18.97	1.74	11.56	8.48	10.39
Al_2O_3	1.25	0.29	2.86	3.10	2.36	2.27	1.86	0.42	2.61	3.48	3.91	1.49
FeO	80.90	55.24	78.27	78.08	75.56	79.88	71.09	66.58	76.80	76.22	79.54	78.84
MnO	1.25	0.38	0.69	0.72	0.84	0.84	1.12	0.72	1.58	0.21	0.29	0.21
MgO	2.15	1.56	5.14	5.22	5.15	4.66	5.28	4.04	7.55	0.04	0.03	0.02
CaO	0.23	0.75	0.05	0.05	0.11	0.21	0.46	0.41	0.37	0.11	0.09	0.09
Na_2O	0.22	0.07	0.15	0.20	0.14	0.08	0.13	0.08	0.20	0.24	0.07	0.13
K_2O	0.05	0.09	0.01	0.02	0.05	0.04	0.02	0.02	0.00	0.00	0.00	0.01

 https://doi.org/10.5281/zenodo.16876847

P_2O_5	0.00	0.62	0.02	0.00	0.05	0.00	0.07	0.05	0.04	0.00	0.02	0.01
Total	89.53	92.90	91.45	91.96	93.15	91.93	92.06	91.60	91.18	92.15	92.68	91.47
Si	0.000	0.033	0.010	0.011	0.022	0.011	0.011	0.020	0.020	0.025	0.012	0.078
Ti	0.062	1.972	0.142	0.150	0.580	0.132	0.391	0.923	0.092	0.786	0.293	2.202
Al	1.120	0.026	0.157	0.169	0.248	0.126	0.097	0.032	0.217	0.371	0.211	0.494
Fe	20.299	3.619	3.062	3.022	5.644	3.148	2.629	3.601	4.520	5.767	3.053	18.571
Mn	20.388	0.025	0.027	0.028	0.063	0.033	0.042	0.040	0.094	0.016	0.011	0.051
Mg	0.557	0.182	0.359	0.360	0.686	0.328	0.348	0.389	0.792	0.006	0.002	0.009
Ca	0.686	0.063	0.003	0.003	0.011	0.011	0.022	0.028	0.028	0.011	0.005	0.028
Na	0.135	0.011	0.014	0.018	0.025	0.007	0.011	0.010	0.028	0.043	0.006	0.072
K	0.081	0.009	0.001	0.001	0.006	0.002	0.001	0.002	0.000	0.000	0.000	0.004
P	0.006	0.021	0.000	0.000	0.002	0.000	0.001	0.001	0.001	0.000	0.000	0.001
Total	23.330	5.961	3.776	3.764	7.286	3.799	3.554	5.045	5.791	7.025	3.593	21.510
#Mg	4.5	4.80	10.48	10.65	10.84	9.42	11.70	9.76	14.91	0.10	0.065	0.048

Based on the results obtained, the chemical composition of iron-titanium minerals in the FeO-TiO_2-Fe_2O_3 classification diagram (Bacon and Hischmann, 1988) is located in the magnetite and titanomagnetite range in all sections (Figure 17).

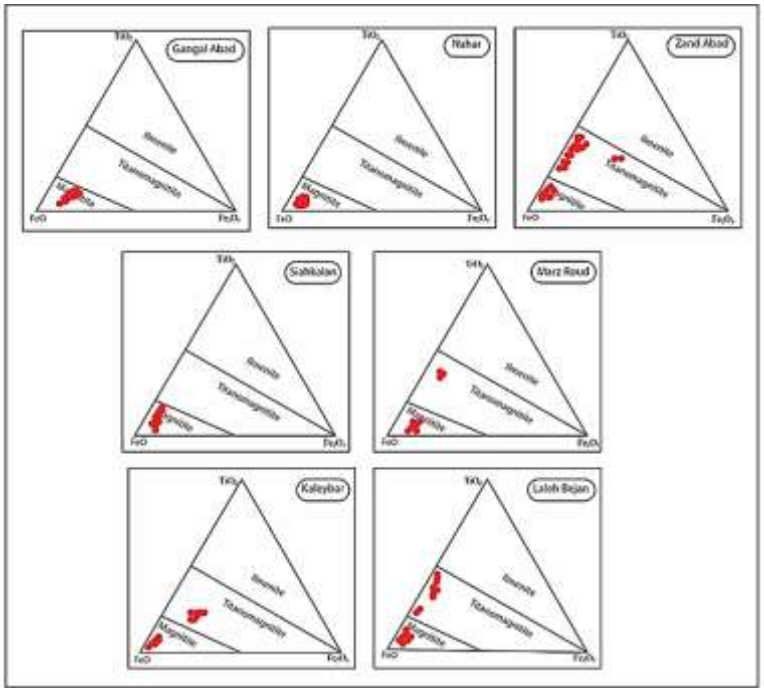

Figure 17: Ternary classification diagram FeO- TiO_2- Fe_2O_3 (Baco and Hischmann, 1988).

- Mineral Thermobarometry: In order to better understand how and why a rock is formed,

 https://doi.org/10.5281/zenodo.16876847

it is necessary to know the conditions during its formation. Experimental and laboratory studies showing the composition of minerals are widely used to identify the temperature-pressure conditions during crystallization (Wells, 1977; Lindsley, 1983; Duchene and Albarede, 1999; Fu et al, 2008; Mollo et al, 2011). In this section, the thermobarometric conditions of crystal-melt equilibrium are discussed and evaluated using the chemical composition of various minerals (such as clinopyroxene, plagioclase, amphibole, and olivine). For the thermobarometry of these minerals, various researchers and scientists have used various methods, especially clinopyroxene, whose chemical composition is very sensitive to changes in the physical conditions of crystallization, and its use in thermobarometric studies is considered a good tool (Kohler and Brey, 1990; Nimis, 1995; Putirka et al, 1996; Soesoo, 1997; Nimis and Ulmer, 1998; Putirka, 1999; Nimis and Taylor, 2000; Putirka et al, 2003; Mollo et al, 2013). In the following section, a description of a number of these methods is presented, and thermobarometric studies have been conducted based on them.

- Clinopyroxene thermobarometry:

- Thermobarometry by the method of (Soesoo, 1997): The chemical composition of pyroxene has been determined from 6 areas: Zandabad, Nahar, Gangalabad, Marzroud, Siahkalan and Kaleybar. So far, various relationships have been proposed to estimate the thermobarometric conditions of pyroxene crystallization (Sayari et al, 2014). In this section, the proposed method (Soesoo, 1997) is used. In this method, with the help of the chemical composition of clinopyroxene, the two parameters XPT and YPT can be used to estimate temperature and pressure through the following equations:

$$X_{PT}= 0.446\ SiO_2+0.187\ TiO_2-0.404\ Al_2O_3+0.346\ FeO_T-0.052\ MnO-0.309\ MgO+0.431\ CaO-0.446\ Na_2O$$

$$Y_{PT}=-0.369\ SiO_2+0.535\ TiO_2-0.317\ Al_2O_3+0.323\ FeO_T+0.235\ MnO-0.516\ MgO-0.167\ CaO-0.153\ Na$$

The calculated XPT and YPT values for some clinopyroxene samples from the study areas are given in Table 6. Based on this method and Figures 18 and 19, the formation of clinopyroxenes from the study areas is estimated to occur in the temperature range of about 1150 to 1220 (±50) ºC and at a pressure of 3 to 13 kbar.

 https://doi.org/10.5281/zenodo.16876847

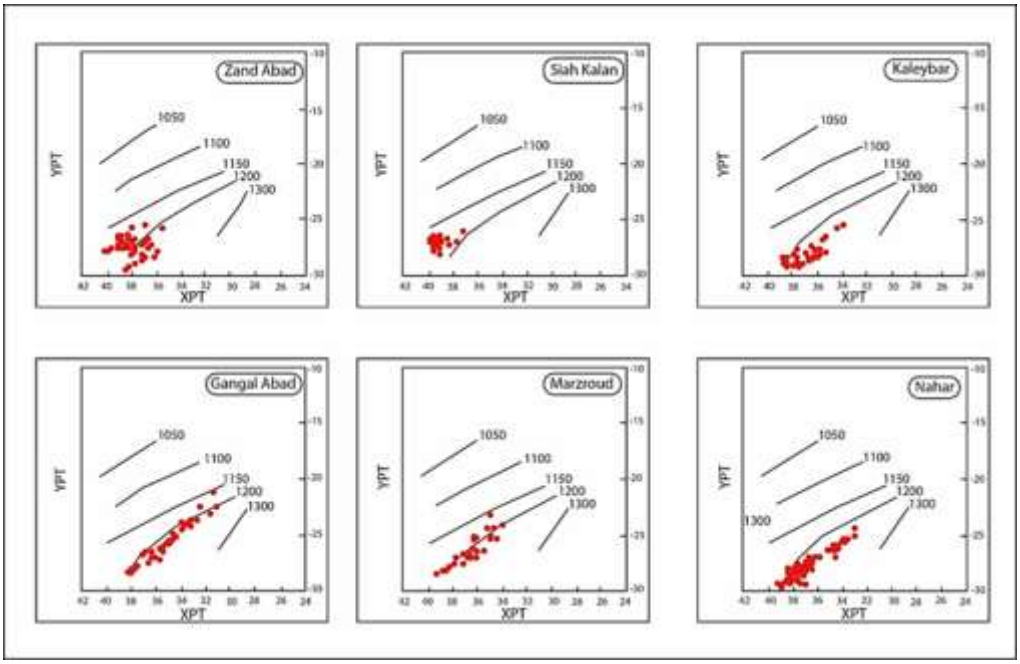

Figure 18: diagram of XPT versus YPT variations for temperature estimation, taken from (Soesoo, 1997).

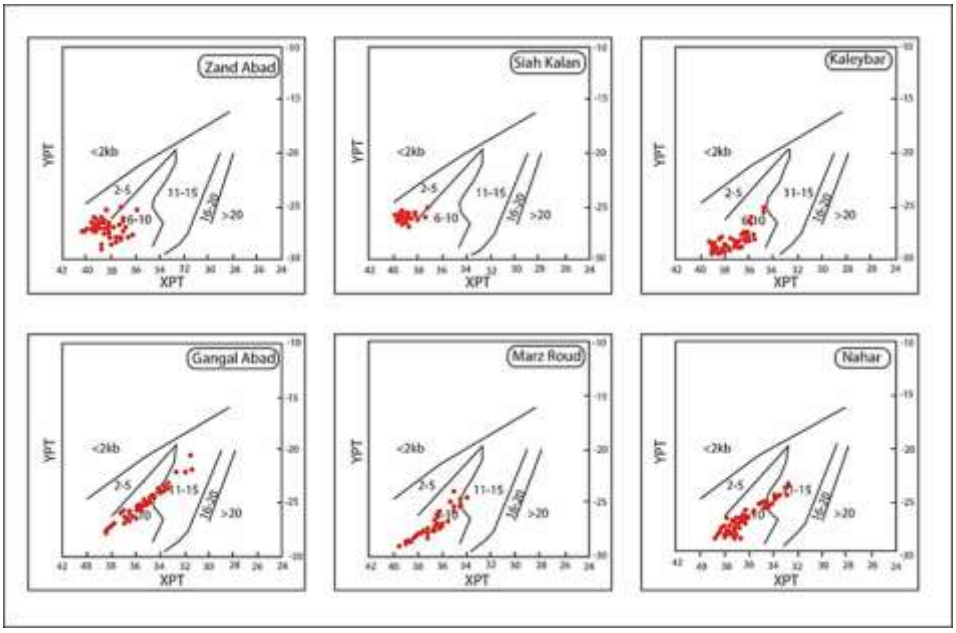

Figure 19: diagram of XPT versus YPT variations for pressure estimation, taken from (Soesoo, 1997).

Table 6: Calculated XPT and YPT for clinopyroxene samples from the study areas

Sample	**BZ**	**BZ**	**BZ**	**BZ**	**NB**	**NB**	**NB**	**NB**	**GB**	**GB**	**GB**	**GB**
X_{PT}	38.14	37.18	39.20	38.43	38.16	37.27	39.08	36.85	35.39	35.44	38.18	36.41
Y_{PT}	-28.14	-27.99	-27.04	-25.99	-28.95	-28.85	-29.79	-28.44	-26.53	-26.43	-28.94	-28.04
Sample	**PBM**	**PBM**	**PBM**	**PBM**	**SB**	**SB**	**SB**	**SB**	**KB**	**KB**	**KB**	**KB**
X_{PT}	38.91	37.92	36.07	37.65	39.29	39.35	39.04	39.09	38.27	38.80	38.94	38.70
Y_{PT}	-29.38	-28.57	-26.41	-28.28	-27.42	-27.37	-26.27	-26.72	-29.86	-29.94	-28.95	-28.95

https://doi.org/10.5281/zenodo.16876847

- Barometry by the method (Akinin et al, 2005): Also, based on this diagram, the estimated pressure value for pyroxene samples is in the range of 7-10 kbar (Figure 20).

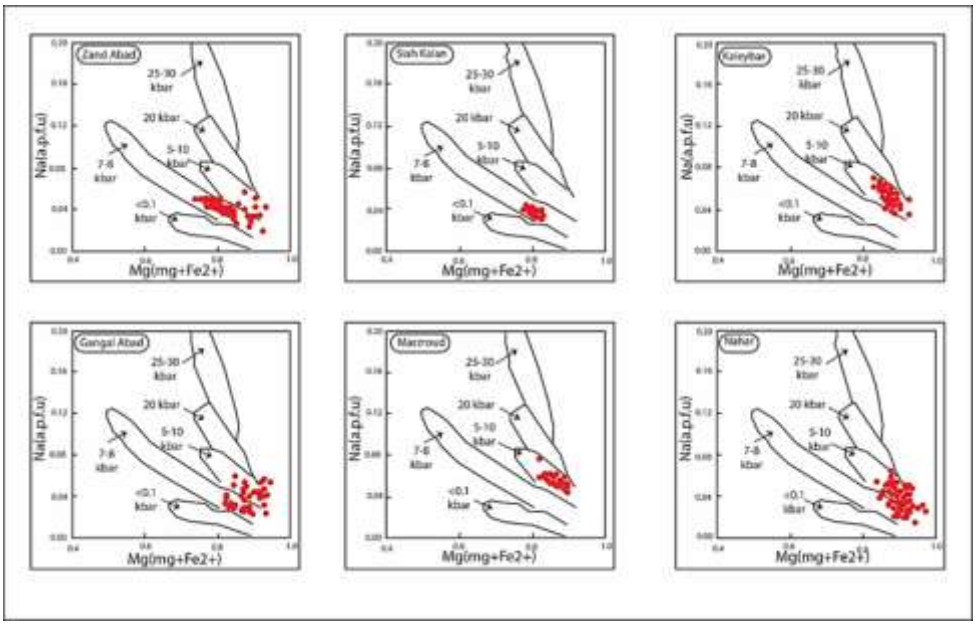

Figure 20: diagram of Mg/(Mg+Fe2+) versus Na variations for estimating the pressure of clinopyroxenes (Akinin et al, 2005)

- Thermometry and barometry by the method of (Putirka et al, 2003; Neave and Putirka, 2017): Thermobarometry of clinopyroxene and symbiotic melt using the method of (Putirka et al, 2003) is used for mafic igneous rocks as well as volcanic rocks. This equation is based on the equilibrium of symbiotic crystal-melt and in addition to the mineral composition, the chemical composition of the melt itself is also used. The temperature and pressure in this equation are based on the crystallization of hedenbergite-diopside and jadeite, which is obtained based on equation 1:

$$\frac{10^4}{T(K)} = 4.60 - 4.37 \times 10^{-1} \ln\left(\frac{X_{Jd}^{Cpx} \times Ca^{liq} \times Fm^{liq}}{DiHd^{Cpx} \times Na^{liq} \times Al^{liq}}\right) - 6.54 \times 10^{-1} \ln(Mg^{liq}) - 3.26 \times 10^{-1}(Na^{liq}) - 6.32 \times 10^{-3}(P(Kbar)) - 0.92 \ln(Si^{liq}) + 2.74 \times 10^{-1} \ln(Jd^{Cpx}) - 273.15$$

$$P(Kbar) = -88.3 + 2.82 \times 10^{-3} T(K) \ln\left(\frac{Ja^{Cpx}}{Na^{liq} \times Al^{liq} \times (Si^{liq})^2}\right) + 2.19 \times 10^{-2} T(K) - 25.1 \ln(Ca^{liq} \times Si^{liq}) + 7.03(Mg^{liq}) + 12.4 \ln(Ca^{liq})$$

$$X_{DiHd}^{liq} = (CaFmSi_2O_6) = X_{Ca}^{Cpx} - X_{CaTs}^{Cpx} - X_{CaTi}^{Cpx} - X_{CrCaTs}^{Cpx}$$

(equation 1)

Based on the above equation, the average temperature obtained for the areas of Zandabad is 1016.23, Nahar 1201.01, Gangalabad 1192.98, Marzroud 1073.81, Siahkalan 1046.39 and Kaleybar 1186.09 ºC, and the average pressure obtained for the areas of Zandabad is 7.05, Nahar 9.83, Gangalabad 10.44, Marzroud 9.41, Siahkalan 3.18 and Kalibar 9.88 kbar. A newer method for obtaining clinopyroxene thermobarometry is the method of Neave and Putirka (2017) based on equations 2 and 3, in which clinopyroxene is in equilibrium with the host melt. The fundamental change in this equation is that the sum of the cationic fractions of Na and K must be considered.

 https://doi.org/10.5281/zenodo.16876847

$$\frac{10^4}{T(\mathrm{K})} = 7.53 - 0.14\ln\left(\frac{X_{Al}^{cpx} X_{CaO}^{liq} X_{Fm}^{liq}}{X_{DiHd}^{cpx} X_{Na}^{liq} X_{Al}^{liq}}\right) + 0.07\left(H_2O^{liq}\right) - 14.9\left(X_{CaO}^{liq} X_{SiO_2}^{liq}\right) - 0.08\ln\left(X_{TiO_2}^{liq}\right) - 3.62\left(X_{NaO_{0.5}}^{liq} + X_{KO_{0.5}}^{liq}\right) - 1.1\left(Mg\#^{liq}\right) - 0.18\ln\left(X_{EnFs}^{cpx}\right) - 0.027P(\mathrm{kbar})$$

(equation 2)

$$P(\mathrm{kbar}) = -26.27 + 39.16\frac{T(\mathrm{K})}{10^4}\ln\left|\frac{X_{Jd}^{cpx}}{X_{NaO_{0.5}}^{liq} X_{AlO_{1.5}}^{liq}\left(X_{SiO_2}^{liq}\right)^2}\right| - 4.22\ln\left(X_{DiHd}^{cpx}\right) + 78.43X_{AlO_{1.5}}^{liq} + 393.81\left(X_{NaO_{0.5}}^{liq} + X_{KO_{0.5}}^{liq}\right)^2$$

(equation 3)

Based on the above equations, the average temperature obtained for the regions of Zandabad is 1026.05, Nahar is 1226.07, Gangalabad is 1194.82, Marzroud is 1105.33, Siahkalan is 1064.39, and Kaleybar is 1211.56 ºC. Also, the pressure obtained for the regions of Zandabad is 4.5, Nahar is in the range of 5.5, Gangalabad is 8.30, Marzroud is 8.43, Siahkalan is 3.0, and Kaleybar is 8.27 kbars. Some of these results are given in Table 7.

Table 7: Thermo-barometric results based on the proposed model (Putirka, 2003; Neave and Putirka, 2017)

Sample	**BZ**	**BZ**	**BZ**	**NB**	**NB**	**NB**	**NB**	**GB**	**GB**	**GB**
Neave and Putirka,T	1047.4	1054.0	1052.8	1195.5	1214.9	1167.4	1182.7	1187.1	1204.1	1191.9
Neave and Putirka, P	3.2	4.3	3.4	5.1	7.0	3.4	4.5	6.7	8.0	6.0
Putirka,T	1041.3	1048.6	1043.6	1233.1	1246.7	1219.7	1229.5	1209.5	1222.0	1207.6
Putirka, P	7.0	8.9	7.1	10.4	12.3	9.5	10.4	10.7	12.1	9.3
Sample	**PBM**	**PBM**	**PBM**	**SB**	**SB**	**SB**	**SB**	**KB**	**KB**	**KB**
Neave and Putirka,T	1101.5	1116.8	1097.8	1080.4	1066.6	1063.3	1078.9	1211.0	1228.6	1221.7
Neave and Putirka, P	7.7	10.0	7.9	3.3	3.0	2.6	4.1	7.8	9.4	8.4
Putirka,T	1067.8	1082.5	1068.2	1058.6	1048.3	1046.6	1056.2	1187.5	1197.4	1188.6
Putirka, P	8.0	11.2	8.7	3.4	3.2	2.9	4.4	9.7	10.9	9.2

- Thermometry and barometry of plagioclase minerals:

- Thermometry and barometry by the method of (Putirka., 2005b): Given the abundance of plagioclase in most igneous rocks, other researchers have also conducted studies in this field (Mathez, 1973; Drake, 1976; Loomis, 1979; Glazner, 1984; Ariskin and Barmina, 1990; Marsh et al, 1990). Then Putirka's (2005b) studies of plagioclase thermometers showed that calibrations (Sugawara, 2001; Ghiorso et al, 2002) provide the most accurate temperature predictors for existing models, but these models perform poorly at lower temperatures (less than 1100°C) and for aqueous systems. It was shown that improvements in temperature estimation can be achieved by using a simpler model using equation 4.

 https://doi.org/10.5281/zenodo.16876847

$$\frac{10^4}{T(\mathrm{K})} = 6.12 + 0.257\ln\left(\frac{X_{An}^{pl}}{X_{CaO}^{liq}\left(X_{AlO_{1.5}}^{liq}\right)^2\left(X_{SiO_2}^{liq}\right)^2}\right) - 3.166\left(X_{CaO}^{liq}\right) - 3.137\left(\frac{X_{AlO_{1.5}}^{liq}}{X_{AlO_{1.5}}^{liq} + X_{SiO_2}^{liq}}\right) + 1.216\left(X_{An}^{pl}\right)^2 - 2.475\times10^{-2}\left(P(\mathrm{kbar})\right) + 0.2166\left(H_2O^{liq}\right) \quad \text{(equation 4)}$$

The above equation has performed well in other experiments (Blundy et al, 2006) and new experiments show high accuracy with an overall regression improvement of about 6°C (Equation 5):

$$\frac{10^4}{T(\mathrm{K})} = 6.4706 + 0.3128\ln\left(\frac{X_{An}^{pl}}{X_{CaO}^{liq}\left(X_{AlO_{1.5}}^{liq}\right)^2\left(X_{SiO_2}^{liq}\right)^2}\right) - 8.103\left(X_{SiO_2}^{liq}\right) + 4.872\left(X_{KO_{0.5}}^{liq}\right) + 1.5346\left(X_{Ab}^{pl}\right)^2 + 8.661\left(X_{SiO_2}^{liq}\right)^2 - 3.341\times10^{-2}\left(P(\mathrm{kbar})\right) + 0.18047\left(H_2O^{liq}\right) \quad \text{(equation 5)}$$

Also, for alkali feldspars, temperature can be represented through two new models based on albite-liquid equilibrium (Equations 6 and 7).

$$\frac{10^4}{T(\mathrm{K})} = 17.3 - 1.03\ln\left(\frac{X_{Ab}^{ab}}{X_{NaO_{0.5}}^{liq}X_{AlO_{1.5}}^{liq}\left(X_{SiO_2}^{liq}\right)^3}\right) - 200\left(X_{CaO}^{liq}\right) - 2.42\left(X_{NaO_{0.5}}^{liq}\right) - 29.8\left(X_{KO_{0.5}}^{liq}\right) + 13500\left(X_{CaO}^{liq} - 0.0037\right)^2 - 550\left(X_{KO_{0.5}}^{liq} - 0.056\right)\left(X_{NaO_{0.5}}^{liq} - 0.089\right) - 0.078P(\mathrm{kbar}) \quad \text{(equation 6)}$$

$$\frac{10^4}{T(\mathrm{K})} = 14.6 + 0.055\left(H_2O(\mathrm{wt\%})\right) - 0.06P(\mathrm{kbar}) - 99.6\left(X_{NaO_{0.5}}^{liq}X_{AlO_{1.5}}^{liq}\right) - 2313\left(X_{CaO}^{liq}X_{AlO_{1.5}}^{liq}\right) + 395\left(X_{KO_{0.5}}^{liq}X_{AlO_{1.5}}^{liq}\right) - 151\left(X_{KO_{0.5}}^{liq}X_{SiO_2}^{liq}\right) + 15037\left(X_{CaO}^{liq}\right)^2 \quad \text{(equation 7)}$$

The average temperatures obtained using the method (Putirka, 2005b) for the areas of Zandabad are 1183.19, Nahar 1192.72, Gangalabad 1176.85, Marzroud 1201.27, Siahkalan 1249.90, Lalehbejan 1221.29 and Kaleybar 1208.58 degrees Celsius. The barometric pressure is also based on the equilibrium between albite, anorthite and the composition of the host melt and is based on the average of 8:

$$P(\mathrm{kbar}) = -42.2 + 4.94\times10^{-2}T(\mathrm{K}) + 1.16\times10^{-2}T(\mathrm{K})\ln\left(\frac{X_{Ab}^{pl}X_{AlO_{1.5}}^{liq}X_{CaO}^{liq}}{X_{An}^{pl}X_{NaO_{0.5}}^{liq}X_{SiO_2}^{liq}}\right) - 382.3\left(X_{SiO_2}^{liq}\right)^2 + 514.2\left(X_{SiO_2}^{liq}\right)^3 - 19.6\ln\left(X_{Ab}^{pl}\right) - 139.8\left(X_{CaO}^{liq}\right) + 287.2\left(X_{NaO_{0.5}}^{liq}\right) + 163.9\left(X_{KO_{0.5}}^{liq}\right) \quad \text{(equation 8)}$$

Based on this equation, the average pressures obtained for the areas of Zandabad are 16.36, Nahar 9.61, Gangalabad 19.87, Marzroud 30.86, Siahkalan 13.79, Lalehbejan 10.15, and Kaleybar 13.84 kbar, some of which are listed in Table 8.

Table 8: Results of thermobarometry of plagioclase minerals using the method (Putirka, 2005b):

 https://doi.org/10.5281/zenodo.16876847

Sample	BZ	BZ	BZ	BZ	NB	NB	NB	GB	GB	GB	PBM
Putirka, T	1166.2	1164.5	1163.0	1195.7	1204.9	1175.3	1189.8	1190.9	1189.4	1190.2	1187.8
Putirka, P	15.7	16.1	16.3	17.4	7.2	11.5	9.3	20.5	19.7	18.2	27.6
Sample	**PBM**	**PBM**	**SB**	**SB**	**SB**	**LB**	**LB**	**LB**	**KB**	**KB**	**KB**
Putirka, T	1180.0	1180.2	1244.7	1242.0	1244.6	1214.9	1248.6	1224.0	1209.9	1209.1	1202.5
Putirka, P	29.5	29.4	13.2	13.8	13.4	12.3	7.6	10.6	13.8	13.3	14.6

- Amphibole thermometry and barometry:

- Thermometry and barometry according to the method (Schmidt, 1992; Vynhal et al, 1991): Barometry is performed based on the AlTotal content in amphiboles according to equation 9 (Schmidt, 1992):

$$P(\pm 0.6\ \text{kbar}) = -3.01 + 4.76\ Al^{Total} \qquad \text{(equation 9)}$$

Also, in order to evaluate possible dependencies between temperature, pressure and chemical composition of amphiboles, equation 10 has been proposed for calculating temperature at pressures of 1 to 20 kbar (Vynhal et al, 1991):

$$T = 25.3\ P + 654.9 \qquad \text{(equation 10)}$$

The temperature and pressure values obtained from equations 8 and 9 are given in Table 9.

Table 9: Pressure and temperature values obtained for amphiboles of the studied areas (Schmidt, 1992; Vynhal et al, 1991)

Sample	BZ	BZ	BZ	BZ	PBM	PBM	PBM	PBM
T	818.86	825.18	834.30	838.66	713.86	719.16	746.89	753.57
P	6.48	6.73	7.09	7.26	5.33	6.54	6.64	6.90
Sample	**LB**	**LB**	**LB**	**LB**	**KB**	**KB**	**KB**	**KB**
T	840.47	819.68	832.66	862.73	864.87	865.56	849.67	836.01
P	7.33	6.51	7.03	8.21	8.30	8.33	7.70	7.16

Based on the calculations, the average pressure value obtained for the Zandabad region is 7.22 kbar and the average temperature value obtained for this region is 842.05 ºC. Also, the average pressure value in the Marzroud region is 6.41 kbar and the average temperature value obtained is 733.37 ºC. The average pressure value in the Lalehbejan region is 7.36 kbar and the average temperature values obtained are 840.98 ºC. The average pressure values in the Kaleybar region are 7.78 kbar and the average temperature values obtained in this region are 851.81 ºC.

- Thermometry and barometry by the method (Putirka, 2016): Various empirical equations have been proposed by various scientists to quantitatively relate the physical and

 https://doi.org/10.5281/zenodo.16876847

chemical conditions of silicate melts in equilibrium with amphibole (including T, P and molten SiO_2) (Ridolfi et al, 2010; Ridolfi and Renzull, 2012; Putirka, 2016). The empirical equations are formulated based on high P-T equilibrium experiments using volcanic rocks as raw materials. In recent studies, the T, P and SiO2 conditions of silicate melts in equilibrium with amphibole have been estimated using empirical equations based on amphibole composition. Although several barometers and geometers have been proposed based on the partitioning of elements between amphibole and plagioclase (Blundy and Holland, 1990; Holland and Blundy, 1994; Molina et al, 2015) and between amphibole and silicate melt (Putirka, 2016), all of them require the assumption of equilibrium between amphibole and other phases. Therefore, if amphibole and other phases are not in equilibrium, these equations will increase the errors associated with P-T estimates. In this study, the T and P conditions of equilibrium with amphibole with symbiotic melt or host rock were calculated using empirical equations based on amphibole composition and referring to the Putirka method (Putirka, 2016) (Equation 11).

$$\begin{aligned} T(^{\circ}C) = {} & 1781 - 132.74 \times \left[Si^{Amp}\right] \\ & + 116.6 \times \left[Ti^{Amp}\right] - 69.41 \\ & \times \left[Fe_t^{Amp}\right] + 101.62 \times \left[Na^{Amp}\right] \end{aligned}$$

(equation 11)

Although (Putirka, 2016) presented pressure-dependent and pressure-independent models, the temperature estimation errors are the same for both models, i.e. the mean and standard deviation of the difference between the estimated and experimental temperatures for the pressure-dependent model are 3.2 °C and 28 °C, respectively, and for the pressure-independent model are 0.4 °C and 30 °C, respectively. Empirical barometric equations based on amphibole composition have been proposed by different scientists (Ridolfi et al, 2010; Ridolfi and Renzull, 2012). The Ridolfi model (Ridolfi et al, 2010) is a function of the aluminum content in amphibole, while the Ridolfi model (Ridolfi and Renzull, 2012) depends on the aluminum content and the concentration of other elements in amphibole (130 MPa < P < 500 MPa) (Equations 12 and 13).

$$\begin{aligned} \ln P\,(\mathrm{MPa}) = {} & 38.723 - (2.6957 \times \mathrm{Si}) - (2.3565 \times \mathrm{Ti}) \\ & - (1.3006 \times \mathrm{Al}) - (2.7780 \times \mathrm{Fe}) \\ & - (2.4838 \times \mathrm{Mg}) - (0.6614 \times \mathrm{Ca}) \\ & - (0.2705 \times \mathrm{Na}) + (0.1117 \times E) \quad (3) \end{aligned}$$

(equation 12)

$$\begin{aligned} P\,(\mathrm{MPa}) = {} & 24023 - (1925.3 \times \mathrm{Si}) - (1720.6 \times \mathrm{Ti}) \\ & - (1478.5 \times \mathrm{Al}) - (1843.2 \times \mathrm{Fe}) \\ & - (1746.9 \times \mathrm{Mg}) - (158.28 \times \mathrm{Ca}) \\ & - (40.444 \times \mathrm{Na}) + (14.389 \times \mathrm{K}). \quad (4 \end{aligned}$$

(equation 13)

Several scientists (Erdmann et al, 2014; Putirka, 2016) have quantitatively examined the models (Ridolfi et al, 2010; Ridolfi and Renzull, 2012) and suggested that the pressures estimated using equations 12 and 13 reflect the composition of the bulk magma. However, (Nagasaki et al, 2017) re-examined the reliability of equations 12 and 13 using a dataset collected from high-pressure-temperature equilibrium experiments selected by Putirka (2016)

 https://doi.org/10.5281/zenodo.16876847

and showed that these equations can be used to approximate pressure estimates with an error of about (±85 MPa). Both equations give similar pressure values. The reliability of amphiboles barometry is still under debate. Based on the above equations, the average temperature values obtained for the Zandabad region are 956.40, for the Marzroud region 917.16, for the Lalehbejan region 954.87, and for the Kaleybar region 966.43 ºC. Also, the average pressure values obtained for the Zandabad region are 7.81, for the Marzroud region 10.06, for the Lalehbejan region 5.13, and for the Kaleybar region 6.85 kbars, the results of which are given in Table 10.

Table 10: Pressure-temperature values obtained for amphiboles in the studied areas using the method (Putirka, 2016)

Sample	**BZ**	**BZ**	**BZ**	**BZ**	**PBM**	**PBM**	**PBM**	**PBM**
T	952.2	987.8	970.1	967.0	853.8	818.3	950.6	968.5
P	7.1	6.6	10.1	8.7	11.5	11.7	8.3	6.7
Sample	**LB**	**LB**	**LB**	**LB**	**KB**	**KB**	**KB**	**KB**
T	940.2	969.4	961.5	967.2	974.3	953.9	980.1	967.1
P	6.6	4.8	5.0	5.1	6.7	7.5	6.2	8.1

- Olivine thermometry by (Beattie, 1993; Putirka, 2007): For the first time, and based on the nickel partitioning, a liquid-olivine thermometer was calibrated (Hakli and Wright, 1967). These efforts were then updated (Leeman and Lindstrom, 1978), and eventually extended to other stages and methods (Petry et al, 1997; Canil, 1999; Righter, 2006). The most recent thermometry studies have focused on the distribution of magnesium between olivine and liquid, and the first calibrations have been performed (Roeden and Emslie, 1970). Another model does not mention the olivine composition as an input, but is grouped due to mathematical similarity and close fit in the output data (Beattie, 1993). The beattie equations are calculated as follows (Equations 14 and 15):

$$T(^{\circ}\mathrm{C}) = \frac{13603 + 4.943\times10^{-7}\left(P(\mathrm{GPa})\times10^{9} - 10^{-5}\right)}{6.26 + 2\ln D_{\mathrm{Mg}}^{ol/liq} + 2\ln[1.5(C_{NM}^{L})] + 2\ln[3(C_{SiO_2}^{L})] - NF} - 273.15$$

(equation 14)

$$D_{\mathrm{Mg}}^{ol/liq} = \frac{0.666 - \left(-0.049X_{\mathrm{MnO}}^{liq} + 0.027X_{\mathrm{FeO}}^{liq}\right)}{X_{\mathrm{MgO}}^{liq} + 0.259X_{\mathrm{MnO}}^{liq} + 0.299X_{\mathrm{FeO}}^{liq}}$$

(equation 15)

The above equation introduces systematic errors at high temperatures and pressures (Beattie, 1993), therefore a correction has been proposed to eliminate such errors according to equation 16, in which the pressure is considered to be equal to 1 kbar, which is used for dry systems (Herzberg and Ohara, 2002).

$$T(^{\circ}\mathrm{C}) = T(^{\circ}\mathrm{C})_{1\mathrm{bar}}^{B93} + 54P(\mathrm{GPa}) - 2P(\mathrm{GPa})^{2}$$

(equation 16)

 https://doi.org/10.5281/zenodo.16876847

ISSN: 0369-8963

In order to use these equations and calibration for aqueous systems, a new calibration has been proposed, the best thermometer of which is according to equation 17 (Putirka, 2007).

$$T(°C) = \{15294.6 + 1318.8P(GPa) + 2.4834[P(GPa)]^2\} / \{8.048 + 2.8352 \ln D_{Mg}^{ol/liq} + 2.097 \ln[1.5(C_{NM}^{L})] + 2.575 \ln[3(C_{SiO_2}^{liq})] - 1.41NF + 0.222H_2O^{liq} + 0.5P(GPa)\}$$

(equation 17)

In this equation, in addition to the crystal composition, the chemical composition of the host melt must also be considered. As can be seen in the equation above, elements such as magnesium, manganese, calcium and iron are used. Experiments involving more than 1200 experimental data have shown that the two best models have been selected (Beattie, 1993 and Putirka et al, 2007). The temperature obtained for the olivines of the Nahar region based on the Beattie equation (1993) is 1337°C and that of the Gangalabad region is 1289°C. Also, the average temperature obtained based on the Putirka equation (2007) is 1316.21°C for the Nahar region and 1261.97°C for the Gangalabad region, and these results are shown in Table 11.

Table 11: Olivine thermometry by the method (Beattie, 1993; Putirka, 2007)

Sample	**NB**	**NB**	**NB**	**NB**	**NB**	**NB**	**NB**	**NB**
Putirka, 2007	1321.3	1320.6	1314.7	1318.2	1312.7	1320.8	1318.5	1314.2
Beattie, 1993	1337.0	1337.0	1337.0	1337.0	1337.0	1337.0	1337.0	1337.0
Sample	**GB**	**GB**	**GB**	**GB**	**GB**	**GB**	**GB**	**GB**
Putirka, 2007	1262.1	1263.4	1260.3	1259.9	1260.4	1254.1	1263.9	1261.1
Beattie, 1993	1289.0	1289.0	1289.0	1289.0	1289.0	1289.0	1289.0	1289.0

- Discussion of thermobarometric results: The rocks studied, as previously discussed, have the composition of basalt, basaltic andesite, trachybasalt, trachyandesitic basalt and trachyandesitic. These melts, both in terms of the percentage of partial melting and in terms of enriched mantle origin, are consistent with a garnet lherzolite mantle origin with 30% partial melting. Certainly, these melts have undergone some amount of transformation (such as fractional crystallization, impurity, mixing, etc.) on their way to the Earth's surface, depending on how fast they and reached the Earth's surface, and are less likely to have the geochemistry of a primary melt. Therefore, it is logical that they undergo some fractional crystallization (i.e., crystallization at great depths and the separation of large crystals such as olivine, plagioclase, pyroxene, and amphibole) on their way to the surface. What has been discussed in this article about thermobarometry has only focused on the crystals present in the rocks under study and at what depth within the Earth these crystals crystallized or reached equilibrium with the symbiotic melt. The results of thermometric calculations of the minerals olivine, plagioclase, and pyroxene indicate temperatures above 1000 ºC. For the pyroxene mineral, based on the studies of Soesoo (1997), the temperature is 1150-1220 ° C, based on the studies of Putirka

https://doi.org/10.5281/zenodo.16876847

(2003), the temperature is 1016.23-1201.01 ° C, and based on the studies of Neave and Putirka (2017), the temperature is 1206.05-1226.07 ° C, which are consistent with each other. For the plagioclase mineral, based on the studies of Putirka (2005b), the temperature is 1176.85-1249.90 ° C. For the mineral olivine, based on the studies of Beattie (1993), the temperature is 1289-1337 ° C, and based on the studies of Putirka (2007), the temperature is 1261.97-1316.21 ° C. For the mineral amphibole, based on the studies of Schmidt (1992), the temperature is 733.37-851.81 ° C, and based on the studies of Putirka (2016), the temperature is about 917.16-954.87 ° C. The results of barometric calculations of plagioclase, which are equal to 10.15-30.86 kbar, indicate that plagioclase crystallization occurs at greater depths and is equivalent to the Earth's mantle. The results of barometric calculations of pyroxene and amphibole indicate crystallization at intermediate pressures and is equivalent to the depth of the middle-lower crust. For pyroxene, based on the studies of Soesoo (1997), the pressure is 3-13 kbar, based on the studies of Akinin (2005), the pressure is 7-10 kbar, based on the studies of Putirka (2005b), the pressure is 3.18-10.44 kbar, and based on the studies of Neave and Putirka (2017), the pressure is 3-8.43 kbar. For amphibole mineral, based on the studies of Schmidt (1992), the pressure is 6.41-7.78 kbar and based on the studies of Putirka (2016), the pressure is 5.13-10.06 kbar. These thermobarometric results are in good agreement with each other and are also consistent with petrographic evidence (non-equilibrium textures such as plagioclase sieve texture, etc.). Therefore, these results can be trusted.

- Whole-rock geology: After microscopic studies, in order to access the geochemical characteristics of the magma forming the rocks of the studied areas, 21 samples were selected for XRF analysis and 19 samples were selected for ICP-Ms analysis and analyzed for oxides of major and trace elements (Tables 12 and 13). Using the results obtained, the type of generating magma, the phenomenon of fractionation, partial crystallization, mixing and magmatic digestion have been discussed and investigated.

Table 12: The results of chemical analysis of the main elements of the studied volcanic rocks

No.	SiO_2	TiO_2	Al_2O_3	Fe_2O_3	MnO	MgO	CaO	Na_2O	K_2O	P_2O_5
BZ2	58.65	0.95	18.36	5.97	0.15	1.51	5.00	3.63	3.23	0.46
BZ3	58.41	0.92	17.73	5.94	0.16	2.21	5.96	3.45	3.09	0.47
KB3	49.65	1.35	15.46	8.24	0.16	4.91	10.52	3.91	1.63	0.95
KB4	49.14	1.55	15.38	8.19	0.14	4.94	10.91	3.93	1.66	0.96
KB6	51.47	0.86	18.06	9.44	0.25	3.77	10.23	3.28	1.38	0.35
KB2A	56.40	0.99	18.85	5.62	0.09	2.65	7.42	4.25	1.79	0.72
KBM5	51.61	1.58	16.78	7.95	0.11	4.11	9.33	3.51	2.18	1.02
NB1	48.96	1.31	14.13	8.96	0.14	8.91	10.07	3.88	1.71	0.67
NB2	57.30	0.87	16.71	6.58	0.14	2.30	6.89	4.29	3.48	0.49
NB3	49.17	1.27	14.20	8.79	0.14	8.80	9.38	3.67	1.63	0.64

 https://doi.org/10.5281/zenodo.16876847

NB4	49.5	1.24	13.69	8.84	0.14	9.99	9.47	3.58	1.40	0.54
GB4	44.57	1.86	15.28	10.15	0.16	7.49	11.23	3.05	1.44	1.22
PBM22	52.04	1.56	15.94	7.47	0.11	4.14	9.07	4.52	2.01	0.95
PBM12	53.76	0.66	18.71	7.62	0.18	2.53	7.23	3.12	3.61	0.28
PBM21	51.25	1.35	17.83	7.43	0.11	4.42	9.46	3.89	1.46	1.02
PBM23	52.38	1.67	15.5	8.46	0.11	4.45	8.55	4.44	2.34	0.79
PBM32	51.36	0.93	16.64	8.71	0.20	3.16	6.28	3.62	3.82	0.37
LB3	53.02	1.02	16.20	7.46	0.11	4.26	8.56	3.58	0.43	0.43
LB4	54.34	1.05	17.45	6.79	0.10	3.60	8.77	4.99	1.45	0.66
SB1	52.01	0.77	19.22	7.52	0.13	2.87	8.23	3.18	1.32	0.12
SB3	53.13	0.76	19.11	8.05	0.13	2.47	7.89	3.54	1.33	0.13

Table 13: Results of chemical analysis of rare and trace elements of studied volcanic rocks

No.	**Ba**	**Ce**	**Co**	**Cr**	**Cs**	**Dy**	**Er**	**Eu**	**Gd**	**Hf**	**La**	**Lu**	**Nb**	**Nd**	**Ni**
BZ2	762	62	16.7	62	0.8	38	1.8	2.03	4.52	3.1	52	0.2	17.1	19.6	25
BZ3	774	67	14	50	0.2	3.5	1.8	2.02	4.09	3.1	53	0.2	19.3	29.6	17
KB3	768	105	21.9	64	<0.5	3.3	1.8	2.44	5.07	2.2	81	0.2	17.4	46	28
KB4	723	103	22.1	58	<0.5	3.2	1.8	2.6	5.01	2	81	0.1	18	44.6	26
KB6	261	20	18.1	48	<0.5	3.9	2.2	1.4	3.32	0.7	19	0.3	5	16.7	7
KB2A	677	77	15.9	47	<0.5	2.5	1.3	1.79	3.94	2.1	68	<0.1	13.8	34.2	19
KBM5	699	89	21.4	58	<0.5	3.1	1.4	2.29	4.65	2.3	69	0.1	15.2	41.5	22
NB1	1023	85	33.4	218	1.2	3.7	1.7	2.39	4.79	2.7	63	0.2	15.6	38.8	156
NB3	1095	78	32.6	236	0.8	3.3	1.6	2.23	4.65	2.6	61	0.2	16	36.6	172
NB4	482	67	32.8	291	1.0	3.0	1.7	1.81	4.12	2.4	51	0.2	14.4	30.08	194
GB4	656	129	31.5	123	1.2	4.6	2.3	3.15	6.64	2.2	97	0.2	23.8	54.8	92
PBM22	1123	28	9.2	30	0.7	3.2	1.7	1.71	3.2	<0.5	25	0.2	8.2	15.2	5
PBM12	686	73	19.6	67	<0.5	2.9	1.4	1.91	4.3	2.2	55	0.1	13.5	35.1	12
PBM21	598	75	17.7	58	<0.5	2.9	1.4	1.98	4.14	2.1	55	0.1	14.6	33.8	7

https://doi.org/10.5281/zenodo.16876847

PBM23	697	74	19.4	60	<0.5	2.9	1.5	2.22	4.22	2.4	54	<0.1	13.7	34.1	12
PBM32	1134	46	20.2	29	1.6	4.0	2.3	2.37	4.2	2.4	36	0.3	6.2	25.9	5
LB3	633	45	12.4	42	<0.5	2.0	1.0	1.19	2.88	1.7	41	<0.1	29.9	18.5	17
LB4	397	47	19	59	1.3	3.4	1.6	1.86	3.91	1.7	40	0.2	13.5	25	31
SB3	320	14	23.5	30	0.8	3.6	2	1.05	2.89	1.4	14	0.3	9.5	10.8	7

Continue the table 13: Results of chemical analysis of rare and trace elements of studied volcanic rocks

No.	**Pb**	**Pr**	**Rb**	**Sc**	**Sm**	**Sr**	**Tb**	**Th**	**U**	**V**	**Y**	**Yb**	**Zn**	**Zr**
BZ2	12	8.27	89	9.7	4.9	750	0.7	6.8	2.2	110	14.8	1.66	77	143
BZ3	12	8.63	93	9	4.8	727	0.7	6.6	2.4	113	15	1.55	76	140
KB3	9	12.43	64	14.4	6.8	2385	0.7	3.5	1.3	181	12.8	1.52	96	116
KB4	7	12.81	62	14.1	6.8	2615	0.7	3.9	1.5	185	12.2	1.43	84	113
KB6	29	3.8	64	16.9	3.5	518	0.7	<0.1	0.4	201	17.5	2.24	125	16
KB2A	7	9.71	64	9	4.9	1274	0.6	3.8	1.3	124	9.2	0.95	65	121
KBM5	8	11.67	64	12.1	6.2	1575	0.7	1.8	0.9	185	10.5	1.29	97	120
NB1	6	10.58	73	16.8	6.7	969	0.7	8.6	2.7	178	13.8	1.62	79	137
NB3	8	9.99	72	16.6	6.3	1077	0.7	7.1	2.2	165	13.3	1.57	78	127
NB4	12	8.57	69	16.9	5.3	798	0.7	5.8	1.9	163	12.7	1.54	84	116
GB4	3	15.35	68	17.8	9.4	2134	0.8	8.4	1.8	210	18.4	2.09	91	139
PBM22	5	4.51	91	7.9	3.3	487	0.6	<0.1	0.7	130	15.4	1.73	67	19
PBM12	10	9.5	66	13.4	4.9	1374	0.7	9.8	0.8	197	10.3	1.31	94	108
PBM21	6	8.92	64	14.1	5.4	1298	0.6	1.7	1.0	193	0.8	1.39	81	112
PBM23	8	9.69	65	13.4	5.3	1363	0.7	1.0	0.9	196	10.2	1.33	89	107
PBM32	11	6.62	111	5.7	5.7	610	0.7	4.1	1.5	204	19.1	2.39	83	112
LB3	8	5.55	62	7.7	2.9	615	0.5	3.1	0.9	85	7.5	0.68	53	85
LB4	7	6.63	55	12.1	4.4	721	0.6	1.4	1.3	127	14	1.56	70	80

 https://doi.org/10.5281/zenodo.16876847

SB3	6	2.8	65	18.8	2.3	426	0.6	<0.1	0.7	207	17.1	2.24	71	65

To accurately determine the exact names of the volcanic rocks and magmatic series studied, the TAS diagram (LeBas et al, 1986) was used (Figure 21, A), which according to this diagram, the rocks of the studied areas are in the range of basalt, basaltic andesite, trachybasalt, basalt-trachyandesite and trachyandesite, and mainly include high-potassium alkaline and calc-alkaline series. In order to determine the aluminum index of igneous rocks, a diagram based on the molar ratio A/NK versus A/CNK was used, which according to this diagram, the volcanic rocks of the studied areas are in the range of metaluminous rocks (Shand, 1943) (Figure 21, B). The REE changes in volcanic rocks and the spider diagrams are normalized to the values proposed by Sun and McDonough, 1989 (Fig. 21, C). In the diagram, the changes have a downward and negative trend, which indicates that the volcanic rocks are enriched in light rare earth elements (LREE) and depleted in heavy rare earth elements (HREE). This feature indicates that the origin of the magma generating the rocks was from deep mantle regions (garnet-lherzolite part) which were later transformed by digestion of crustal rocks, mixing or contamination. If the garnet crystal is separated from the magma in the early stages of crystallization or is not included in the melting process, the remaining magma will be depleted in heavy rare earth elements and enriched in light rare earth elements (Machado et al, 2005).

The negative TNT (Ti, Nb, Ta) anomaly, which is clearly visible in the studied samples, can be related to different levels of contamination. Also, low TNT values can be the result of the presence of Fe-Ti oxides or Nb-Ti-bearing minerals in the remnants of the parent magma at the reservoir site (Pearce and Parkinson, 1993). The presence of a positive Pb anomaly and a negative K anomaly can be considered as contamination of magma with crustal materials (due to high Pb concentration), mixing of magma, the presence of alteration or their high mobility (Rollinson, 1993).

The La/Sm versus La diagram has been used to calculate the extent of partial melting in the studied areas (Aldanmaz et al, 2000). By comparing the composition of lavas and the composition of magmas derived from spinel or garnet-bearing lherzolites, the degree of partial melting and the nature of the source mantle can be determined. The studied samples show a similar composition to magmas derived from enriched mantle in terms of La and Sm elements and are on a consistent trend of up to 30% partial melting of garnet lherzolite (Fig. 21, D).

In the three-variable diagrams (Muller and Groves, 1997), which are characterized by the variables (La-10Hf-TiO2/100) and (3Zr-50Nb-Ce/P2O5), continental arcs are separated from arc islands (Fig. 21, E) and then the post-collisional arc position is distinguished from continental arcs (Fig. 21, F). In these diagrams, all samples are located within the range of continental arcs and post-collisional arcs. Perhaps the reason for this is that the volcanic rocks of the studied areas were formed in the post-collisional stage and in connection with the development of the extensional phase.

 https://doi.org/10.5281/zenodo.16876847

ISSN: 0369-8963

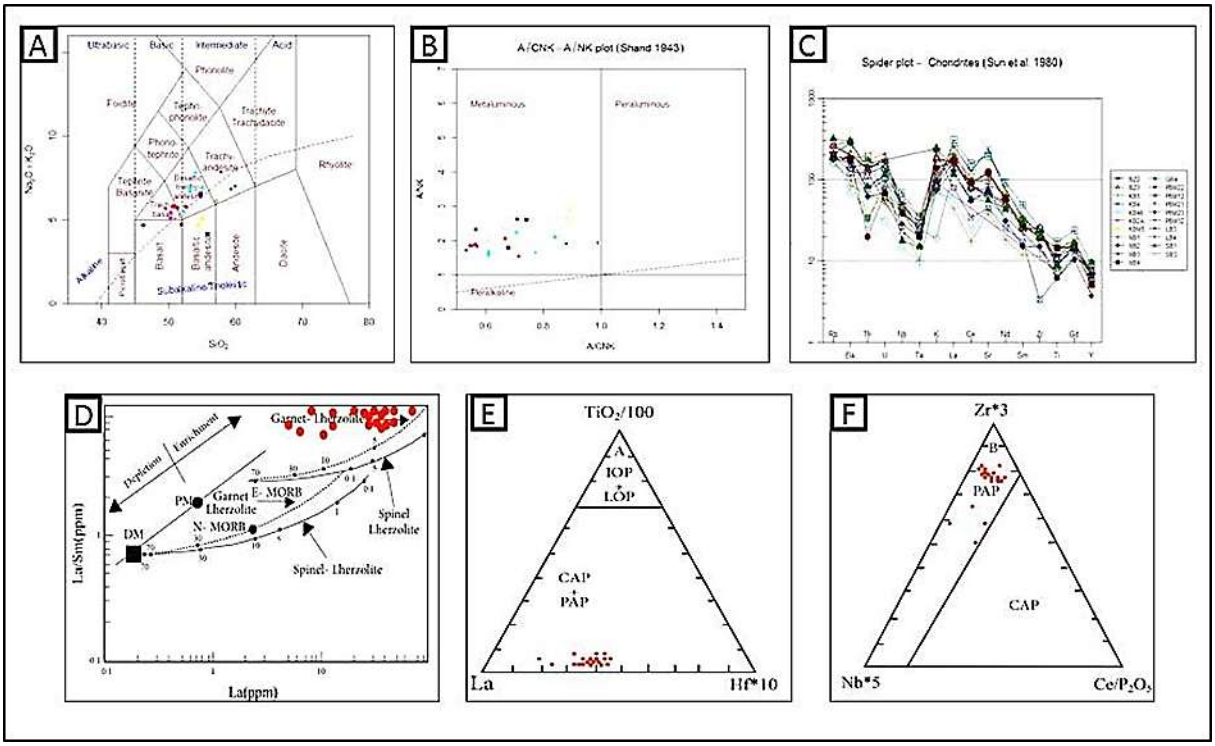

Figure 21: A) Classification of rocks in Kaleybar-Ahar-Varzghan regions based on TAS diagram.
B) A/NK vs. A/CNK molar ratio diagram in order to determine the aluminum index of igneous rocks.
C) Spider diagram of the group of rare elements for the rocks of the studied areas.
D) Diagram of La versus La/Sm in order to calculate the amount of partial melting.
E) diagnostic chart for volcanic rocks based on unconventional rare elements, where the samples are located in the continental arcs.
F) diagnostic diagram based on rare elements, all samples are placed in the range of arcs after impact.

In the Ce/Pb vs. MgO plot (Fig. 22, A) (Furman, 2007), the samples fall within the crustal-contaminated range. The average Ce/Pb ratio in oceanic basalts (OIB and MORB) is about 25 (Hofmann et al., 1986), which is considerably higher than the average value for continental crust (the Ce/Pb ratio in continental crust is 3.2 and the Pb content is 20) (Taylor and Mclennon., 1985). In the diagram, the curve between these two areas represents the boundaries of the OIB and the upper crust (Norman and Garcia., 1999), and according to this diagram (Figure 22, B), the studied samples are located around this curve (Alici et al., 2002), which could indicate the participation of the upper continental crust in the magma forming the studied rocks.

https://doi.org/10.5281/zenodo.16876847

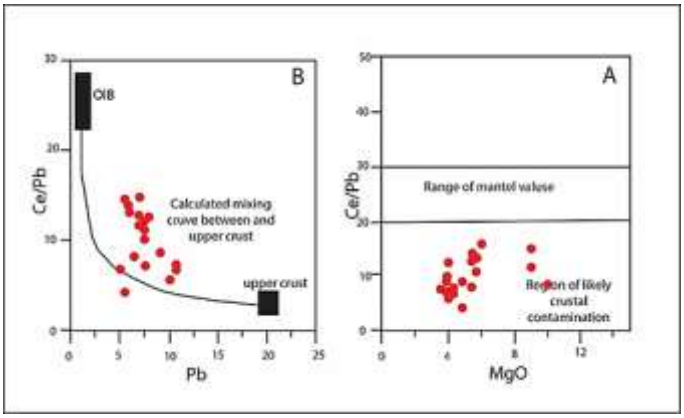

Figure 22: The position of the samples studied in the diagram change with the continental shell pollution

A) diagram Ce/Pb to MgO (Furman, 2007), B) diagram Ce/Pb to Pb (Hofmann et al, 1986).

In all global tectonic maps, Iran is considered part of the active continental margins and part of the continent-continent collision zone of the Alpine-Himalayan orogenic belt. Various theories have been proposed about the magmatic activities of Iran since the Tertiary. Some of these theories are based on subduction models in which the subduction of the Neotethys oceanic crust under the Iranian plate has been proposed. The subduction of the Neotethys Ocean in the Middle Cretaceous beneath the Iranian continental plate caused metasomatism of the lithospheric mantle above the subducting plate and enrichment of the lithospheric mantle (Ghasemi and Talbot, 2006). As subduction continues, the subducting plate becomes steeper and fractures and detachments occur in part of this plate. Fracture of the subducting plate beneath eastern Anatolia has been reported for 12 million years and in the east (northern Zagros) for more than 30 million years. The plate fracture started in the northern Zagros about 30 million years ago and reached Anatolia by 12 million years ago with displacement along the suture zone. In this model, the upwelling of mantle plumes facilitated the melting of metasomatized mantle (Hafkenscheid et al, 2006) and then the Neotethys Ocean was completely closed during the Upper Cretaceous (Searle and Cox, 1999) which finally led to the dominance of a tensile regime in the Iranian Plate during the Eocene and the development of extension along major faults and fractures, which subsequently led to the development of volcanic activity in northwestern Iran and adjacent areas.

- Conclusion: The studied areas are located in the counties of Kaleybar, Ahar and Varzeghan in East Azerbaijan province and northwest of Iran and are located in the Alborz-Azerbaijan zone. The main minerals of these rocks are plagioclase, clinopyroxene, amphibole, olivine and the minor minerals include apatite, quartz and opac minerals. The characteristic textures of the rocks are microlithic porphyritic, hyaloporphyric and porphyric, glomeroporphyritic and trachytic. Data from the point analysis of clinopyroxenes indicate the type of augite and diopside composition, which is alkaline and subalkaline in nature, indicating their igneous origin, and the magnesium number indicates their formation in the primary magma. The chemistry of clinopyroxenes indicates their formation environment in high oxygen fugacity, low to moderate pressures, and the presence of magma water content of less than 10 kbar water barometer. The mineral chemistry of plagioclases, as the most abundant mineral

 https://doi.org/10.5281/zenodo.16876847

both in the form of phenocrysts and as microlites of the type andesine, bitonite, labradorite, and oligoclase.

The weight percentage of FeO versus the molar percentage of anorthite and plagioclase indicates the occurrence of these minerals in mixed conditions, which is consistent with the presence of unbalanced textures such as sieves and... The mineral chemistry of amphiboles indicates the type of composition of pargasite and scharmakite, which are alkaline-subalkaline and subalkaline in nature. The mineral chemistry of olivines in the studied areas is of the chrysolite type and iron-titanium oxides are of the magnetite and titanomagnetite types.

Thermometric calculations have been made for the minerals olivine, plagioclase, pyroxene and amphibole. Thermobarometric calculations based on the chemical composition of the mineral pyroxene show a temperature of 1016.23-1226.07°C and a pressure of 3-13 kbar. Thermobarometric calculations based on the chemical composition of the mineral plagioclase show a temperature of 1176.85-1249.90°C and a pressure of 10.15-30.86 kbar. Thermobarometric calculations of amphibole mineral show temperature of 733.37-954.87 ºC and pressure of 5.13-10.06 kbar. Thermobarometric calculations based on chemical composition of olivine mineral show temperature of 1261.97-1337 ºC. Barometric calculations of pyroxene and amphibole indicate crystallization at medium pressures and equivalent to the depth of the middle-lower crust, and barometric calculations of plagioclase indicate crystallization at greater depths and equivalent to the Earth's mantle.

The composition of the studied rocks is basalt, basaltic andesite, trachybasalt, basalt-trachyandesite and trachyandesite, which belong to the high-potassium alkaline and calc-alkaline magmatic series and are also located in the range of metaluminous rocks. The studied samples show enrichment in light rare earth elements (LREE) and depletion in heavy rare earth elements (HREE), indicating that the magma producing the rocks originates from deep mantle regions and is consistent with up to 30% partial melting of garnet lherzolite. he negative TNT (Ti, Nb, Ta) anomaly can be related to different levels of contamination, the presence of Fe-Ti oxides or Nb-Ti-bearing minerals in the remnants of the parent magma at the reservoir site, and the positive Pb anomaly and the negative K anomaly can be considered related to the contamination of magma with crustal materials (due to high Pb concentration), magma mixing, the presence of alteration or their high mobility. The tectonic environment of the studied samples, in the three-variable diagrams, is located in the area of post-collisional volcanic arcs.

Refrences:

Akinin, V.V., Sobolev, A.V., Ntaflos, T., and Richter, W., 2005. Clinopyroxene megacrysts from Enmelen mela nephelinitic volcanoes (Chukchi Peninsula, Russia): application to composition and evolution of mantle melts. Contributions to Mineralogy and Petrology, 150, 85–101. http://www.doi.org/10.1007/s00410-005-0007-x.

Aldanmaz, E., Pearce, J.A., Thirlwall, M.F., Mitchell, J.G., 2000. Petrigenetic evolution of late Cenozoic, post collision volcanism in western Anatolia, Tirkey, Journal of volcanology and geothermal Reasearch, 102: 67-97.

 https://doi.org/10.5281/zenodo.16876847

Alici, P., Temel, A., Gourgaurd, A., 2002. Pb- Nd- Sr isotope and trace element geochemistry of Quaternary extention- related alkaline volcanism: a case study of Kula region (western Anatolia Turkey), J. Volcanol. Geoth. Res. 115(3), 487- 510.

Allen, M.B., Armstrong, H.A., 2008. Arabia–Eurasia collision and the forcing of mid-Cenozoic global cooling. Palaeogeography, Palaeoclimatology, Palaeoecology 265, 52-58.

Allen, M.B., Kheirkhah, M., Nill, I., Emami, M.H., Mcleod, C., 2013. Generation of arc and within-plate chemical signatures in collision zone magmatism: Quaternary lavas from Kurdistan province, Iran. Journal of Petrology 54, 887–911.

Amel, N., 2007. Petrology and petrogenesis of Plio-Quaternary igneous rocks of Azerbaijan, PhD thesis, Tabriz University, 188 p. [In Persian].

Aoki, K., Shiba, I., 1973. Pyroxenes from lherzolite inclusions of Itinom e-Gata, Japan, Lithos 6: 41-51.

Ariskin, AA., Barmina, GS., 1990. Equilibria thermometry between plagioclases and basalt or andesitemagmas. Geochem Int 27:129-134.

Bacon C.R., Hirschmann, M.M., 1988. “Mg/Mn partitioning as a test for equilibrium between coexisting Fe-Ti oxides” Am. Mineral, 73(1-2), 57-61.

Bavali, K., Motaghi, K., Sobouti, F., Ghods, A., Abbasi, M., Priestley, K., Mortezanejad, G., Rezaeian, M. 2016. Lithospheric Structure beneath NW Iran Using Regional and Teleseismic Travel- time Tomography, Physics of the Earth and Planetary Interiors, PEPI 5897.

Beattie, P., 1993. Olivine-melt and orthopyroxene-melt equilibria. Contrib Mineral Petrol 115:103-111.

Berberian, M., King, G.C.P., 1981. Towards a paleogeography and tectonic evolution of Iran. Canadian journal of Earth Science, vol. 18 No. 2: 210-265.

Beyarslan, M., Lın, Y.-C., Bingöl, A.F., Chung, S.L., 2016. Zircon U-Pb age and geochemical constraints on the origin and tectonic implication of Cadomian (Ediacaran-Early Cambrian) magmatism in SE Turkey, Journal of Asian Earth Sciences 130, 223-238.

Blundy, J., Cashman, K., Humphreys, M., 2006. Magma heating by decompression-driven crystallizationbeneath andesite volcanoes. Nature 443:76-80.

Blundy, J.D., Holland, T.J.B., 1990. Calcic amphibole equilibria and a new amphibole-plagioclase geothermometer. Contrib Miner Petrol, 104(2):208–224.

Bons, P. D., Elburg, M. A., Gomez-Rivas, E., 2012. A review of the formation of tectonic veins and their microstructures, Journal of Structural Geology, 43, 33-62.

Botcharnikov, R. E., Koepke, J., Holtz, F., McCammon, C., Wilke, M., 2005. The effect of water activity on the oxidation and structural state of Fe in a ferro-basaltic melt, Geochimica et Cosmochimica Acta, 69: 5071-5085.

Bowen, N.L., 1928. The Evolution of the IgneousRocks, Princeton University Press, Princeton, N.J., 334 pp.

Canil, D., 1999. The Ni-in-garnet geothermometer: calibration at natural abundances. Contrib MineralPetrol, 136:240-246.

Chiu, H.Y., Chung, S.L., Zarrinkoub, M. H., Mohammadi, S. S., Khatib, M. M., and Iizuka, Y., 2013. Zircon U–Pb age constraints from Iran on the magmatic evolution related to Neotethyan subduction and Zagros orogeny: Lithos, v. 162–163, p. 70–87, 2013.01.006.

Deer, W.A., Howie R.A., Zussman, J., 1992. An introduction to the rock forming minerals, Longman Scientific Technical, New York, 528 p.

Deer, W.A., Howie, R.A., Zussman, J., 1991. An Introduction to the Rock–forming minerals, Longman, London, 528 p.

 https://doi.org/10.5281/zenodo.16876847

Dewey, J.F., Hempton, M.R., Kidd, W.S.F., Saroglu, F., Sengor, A.M.C., 1986. Shortening of continental lithosphere: The neotectonics of eastern Anatolia- a young collision zone in Collision Tectonic Geological Society special publications, No: 19 editted by M.P. Coward and A.C. Res,, 3-36.

Dilek, Y., Altunkaynak, S., 2009. Geochemical and temporal evolution of Cenozoic magmatism in western Turkey: mantle response to collision, slab breakoff, and lithospheric tearing in an orogenic belt. In: van Hinsbergen, D.J.J., Edwards, M.A., Govers, R. (Eds.), Geodynamics of Collision and Collapse at the Africa–Arabia–Eurasia Subduction Zone. Geological Society of London Special Publication, pp. 213–234.

Dilek, Y., Imamverdiyev, N., Altunkaynak, S., 2010. Geochemistry and tectonics of Cenozoic volcanism in the Lesser Caucasus (Azerbaijan) and the peri-Arabian region: collision-induced mantle dynamics and its magmatic fingerprint. International Geology Review 52, 536–578.

Drake, M.J., 1976. Plagioclase-melt equilibria. Geochim Cosmochim Acta, 40:457-465.

Duchene, S., and Albarede, F., 1999. Simulated garnet-clinopyroxene geothermometry of eclogites. Contributions to Mineralogy and Petrology 135(1): 75-91.

Elitok, O., Ozgur, N., Druppel, K., Dilek, Y., Platevoet, B., Guillou, H., Poisson, A., Scaillet, S., Satir, M., Siebel, W., Bardintzeff, J.M., Deniel, H., Yilmaz, K., 2010. Origin and geodynamic evolution of late Cenozoic potassium-rich volcanism in the Isparta area, southwestern Turkey. International Geology Review 52, 454–504.

Erdmann, S., Martel, C., Pichavant, M., Kushnir, A., 2014. Amphibole as an archivist of magmatic crystallization conditions: problems, potential, and implications for inferring magma storage prior to the paroxysmal 2010 eruption of Mount Merapi, Indonesia. Contrib Mineral Petrol 167:1016.

France, L., Ildefonse, B., Koepke, J., Bech, F., 2010. A new method to estimate the oxidation state of basaltic series from microprobe analyses, Journal of Volcanology and Geothermal Research, 189: 340-346.

Frost, A., Frost, C., 2014, Essentials of Igneous and Metamorphic Petrology, 32 Avenue of the Americas, New York, NY 10013-2473, USA, Cambridge University Press is part of the University of Cambridge, Royal Holloway University of London.

Fu, B., Page, F.Z., Cavosie, A. J., Fournelle, J., Kita, N.T., Lackey, J.S., Wilde, S.A., Valley, J.W., 2008. Ti-in-zircon thermometry: applications and limitations. Contributions to Mineralogy and Petrology 156(2): 197-215.

Furman, T., 2007. Geochemistry of East African Rift basalts: An overview, Journal of African Earth Sciences, 48: 147-160.

Ghasemi, A., Talbot, C.J., 2006. A new tectonic scenario for the Sanandaj-Sirjan Zone (Iran). Journal of Asian Earth Sciences, 26: 683–693.

Ghiorso, MS., Hirschmann, MM., Reiners, PW., Kress, VC III., 2002. The pMELTS: a revision of MELTSfor improved calculation of phase relations and major element partitioning related to partialmeltingofthemantleto3 GPa. Geochem Geophys Geosyst, 3:1-36, 10.1029/2001GC000217.

Glazner, A.F., 1984. Activities of olivine and plagioclase components in silicate melts and their applicationto geothermometry. Contrib Mineral Petrol, 88:260-268.

Hafkenscheid, E.,Wortel, M.J.R., Spakman,W., 2006. Subduction history of the Tethyan region derived from seismic tomography and tectonic reconstructions, Journal of Geophysical Research Solid Earth 111 (B8) (Art. No. B08401).

Hakli, T.A., Wright, T.L., 1967. The fractionation of nickel between olivine and augite as a geothermometer. Geochim Cosmochim Acta, 31:877-884.

Har, N., 2005. Reaction coronas around quartz xenocrysts in the basaltic andesite from Detunata (Apuseni Mountains. Romania), Geologica Carpathica, 56(4), 369- 378.

 https://doi.org/10.5281/zenodo.16876847

Helz, R.T., 1973. Phase relations of basalts in their melting ranges at pH2O=5 kb as a function of oxygen fugacity, Part I, mafic phases, Journal of Petrology 14: 249-302.

Herzberg, C., O'Hara, M.J., 2002. Plume-associated ultramafic magmas off Phanerozoic age. J Petrol,43:1857-1883.

Holland, T., Blundy, J., 1994. Non-ideal interactions in calcic amphiboles and their bearing on amphiboleplagioclase thermometry. Contrib Miner Petrol 116(4):433–447.

Innocenti, F., Manneti, P., Mazzuoli, R., Pasquare, G., Villari, L., 1981. Neogene and Quaternary volcanism in the eastern Miditerranean.Time-Space distribution and Geotentonic implication Proc. Inter Confrence Sedimentary Basins of Mediterranean Margins, Urbino, Italy.

Kaislaniemi, L., van Hunen, J., Allen, M.B., Neill, I., 2014, Sublithospheric small-scale convection – A mechanism for collision magmatism. Geology 42, 291–294.

Keskin, M., Pearce, J.A., Mitchell, J.G., 1998. Volcano-Stratigraphy and geochemistry of collision – related volcanism on the Erzurum-Kars plateau North eastern Turkey, J. Vol. Geotherm. Res., 85(1-4): 355-404.

Keskin, M., 2003. Magma generation by slab steepening and breakoff beneath a subduction-accretion complex: An alternative model for collision-related volcanism in Eastern Anatolia, Turkey. Geophysical Research Letters 30, 8046.

Keskin, M., 2005. Domal uplift and volcanism in a collision zone without a mantle plume: Evidence from Eastern Anatolia. M.P.O., Uni. Is. 1-45.

Kheirkhah, M., Allen,M., Emami, M., 2009. Quaternary syn-collision magmatism from the Iran–Turkey borderlands. Journal of Volcanology andGeothermal Research 182, 1–12.

Kohler, T.P., Brey, G.P., 1990. Calcium exchange between olivine and clinopyroxene calibrated as a geothermobarometer for natural peridotites from 2 to 60 kb with applications. Geochimica et Cosmochimica Acta 54(9): 2375-2388.

Kress, V.C., Carmichael, I.S.E., 1991. The compressibility of silicate liquids containing Fe2O3 and the effect of composition, temperature, oxygen fugacity and pressure on their redox states, Contributions to Mineralogy and Petrology, 108: 82-92.

Leake, B.E., Wolley, R., Arps, C.E.S., Birch, W.D., Gilbert, M.C., Grice, J.D., Hawthorn, F.C., Kato, A., Kisch, H.J., Krivovichev, V.G., 1997. Nomenclature of amphiboles: report of the subcommittee on amphiboles of the international mineralogical association commission on new minerals and mineral names, Canadian Mineralogist, 35: 219-246.

Le Bas, M.J., 1962. The role of aluminum in igneous clinopyroxenes with relation to their parentage, American journal of science 260, 267-288. https://doi.org/10.2475/AJS.260.4.267.

Lechmann, A., Burg, J,P., Ulmer, P., Guillong, M., Faridi, M., 2018. Metasomatized mantle as the source of Mid-Miocene-Quaternary volcanism in NW-Iranian Azerbaijan: Geochronological and geochemical evidence, Lithos 304–307 (2018) 311–328.

Leeman, WP., Lindstrom, DJ., 1978. Partitioning of Ni2+ between basaltic and synthetic melts andolivines–an experimental study. Geochim Cosmochim Acta, 42:801-816.

Leterrier, J., Maury, R.C., Thonon, P., Girard, D., Marchal, M., 1982. Clinopyroxene composition as a method of identification of the magmatic affinities of paleo-volcanic series. Earth and Planetary Science Letters 59 139-154. https://doi.org/10.1016/0012-821X(82)90122-4.

Lindsley, D.H., 1983. Pyroxene thermometry. American Mineralogist 68(5-6): 477-493. McKenzie, D. and O'Nions, R. K. (1995). The Source Regions of Ocean Island Basalts. Journal of Petrology 36(1): 133-159.

Lin, Y., Chung, S, L., Feyzi B., Yang, L., Okrostsvaridze, A., Pang, K, N., Lee, H, Y., Lin, T, H., 2020. Diachronous initiation of post-collisional magmatism in the Arabia-Eurasia collision zone, Journal of Lithos, S0024-4937(20)30031-1.

Loomis, TP., 1979. An empirical model for plagioclase equilibrium in hydrous melts. Geochim CosmochimActa, 43:1753-1759.

Machado, A., Lima, E.F., Chemale, J.F., Morta, D., Oteiza, O., Almeida, D.P.M., Figueiredo, A.M.G., Alexandre, F.M., Urrutia J.L., 2005. Geochemistry constraints of Mesozoic-Cenozoic calcalkaline magmatism in the South Shetland arc, Antarctica, Journal of Earth Science, 18: 407-425.

Marsh, BD., Fournelle, J., Myers, JD., Chou, I-M., 1990. On plagioclase thermometry in island-arc rocks: experiments and theory. *In:* Fluid-Mineral interactions: A Tribute to H.P. Eugster. Spencer,RJ,Chou,I-M, (eds) Geochemical Society Special Publication 2:65-83.

Mathez, E.A., 1973. Refinement of the Kudo-Weill plagioclase thermometer and its applications tobasalticrocks. Contrib Mineral Petrol 41:61-72.

McBirney, A.R., 2007. Igneous petrology. 3rd edition, Jones and Bartlett Learning, Burlington, Canada.

McQuarrie, N., Van Hinsbergen, D.J., 2013. Retrodeforming the Arabia-Eurasia collision zone: Age of collision versus magnitude of continental subduction. Geology 41, 315-318.

Mitchel, J., and Westaway, R., 1999. Choronology of Neogene and Quaternary uplift and magmatism in the Caucasus from K-Ar dating of volcanism in Armenia, Tectonophysics, 304, 157-186.

Moayyed, M., 2002. A new perspective on Neotethys formation and its relationship with Tertiary magmatism of Urmia-Dokhtar and Western Alborz zones-Azerbaijan, Proceedings of the 6th National Geological Conference, Shahid Bahonar University, Kerman, pp. 374-378. [In Persian].

Moghadam, H.S., Ghorbani, G., Khedr, M.Z., Fazlnia, N., Chiaradia, M., Eyuboglu, Y., Santosh, M., Francisco, C.G., Martinez, M.L., Gourgaud, A., Arai, S., 2014. Late Miocene K-rich volcanism in the Eslamieh Peninsula (Saray), NW Iran: implications for geodynamic evolution of the Turkish–Iranian High Plateau. Gondwana Research 26, 1028–1050.

Molina, J., Scarrow, J., Montero, P.G., Bea, F., 2009. High-Ti amphibole as a petrogenetic indicator of magma chemistry: evidence for mildly alkalic-hybrid melts during evolution of Variscan basic-ultrabasic magmatism of Central Iberia, Contribution to Mineralogy and Petrology, 158: 69-98.

Molina, J.F., Moreno, J.A., Castro, A., Rodríguez, C., Fershtater, G.B., 2015. Calcic amphibole thermobarometry in etamorphic and igneous rocks: new calibrations based on plagioclase/amphibole Al-Si partitioning and amphibole/liquid Mg partitioning. Lithos 232:286–305.

Mollo, S., Putirka, K., Iezzi, G., Del Gaudio, P., Scarlato, P., 2011. Plagioclase–melt (dis)equilibrium due to cooling dynamics: Implications for thermometry, barometry and hygrometry. Lithos 125(1–2): 221-235.

Mollo, S., Putirka, K., Misiti, V., Soligo, M., Scarlato, P., 2013. A new test for equilibrium based on clinopyroxene–melt pairs: Clues on the solidification temperatures of Etnean alkaline melts at post-eruptive conditions. Chemical Geology 352: 92-100.

Moretti, R., 2005. Polymerization, basicity, oxidation state and their role in ionic modelling of silicate melts, Geophysics, 48: 583-608.

Morimoto, N.J., Fabrice, A., Ferguson, I.V., Ginzburg, M., Ross, F.A., Seifert, J., Zussman, K., Aoki., Gottardi, G., 1988. Nomenclature of pyroxene, Mineralogical Magazine, 52: 535-555.

Muller, D., Groves, D.I., 1997. Potassic Igneous rocks and associated gold-copper ineralization, Earth sciences, 56: 238.

Nagasaki, S., Ishibashi, H., Suwa, Y., Yasuda, A., Hokanishi, N., Ohkura, T., Takemura, K., 2017. Magma reservoir conditions beneath Tsurumi volcano, SW Japan: evidence from amphibole thermobarometry and seismicity. Lithos 278–281:153–165.

Neave, D.A., Putirka, K.D., 2017. A new clinopyroxene-liquid barometer, and implications for magma storage pressures under Icelandic rift zones, (April, vol. 102, p. 777–794,

 https://doi.org/10.5281/zenodo.16876847

2017.Article,DOI:http://dx.doi.org/10.2138/am-2017-5968.Erratum,DOI:http://dx.doi.org/10.2138/am-2017-E1021232).

Nimis, P., 1995. A clinopyroxene geobarometer for basaltic systems based on crystalstructure modeling. Contributions to Mineralogy and Petrology 121(2): 115-125.

Nimis, P., Ulmer, P., 1998. Clinopyroxene geobarometry of magmatic rocks Part 1: An expanded structural geobarometer for anhydrous and hydrous, basic and ultrabasic systems. Contributions to Mineralogy and Petrology 133(1-2): 122-135.

Nimis, P., Taylor, W.R., 2000. Single clinopyroxene thermobarometry for garnet peridotites. Part I. Calibration and testing of a Cr-in-Cpx barometer and an enstatite-in-Cpx thermometer. Contributions to Mineralogy and Petrology 139(5): 541-554.

Nixon, G, T., & Pearce, T, HG., 1987. Laser-interferomety study of oscillatory zoning in plagioclase: the record of magma mixing and phenocryst recycling in calc-alkaline magma chambers, Iztaccihuatl volcano, Mexico, Am, Min., 72, 1144-62.

Norman, M., Garcia, M.O., 1999. Primitive magmas and source characteristics of the Hawaiian plume: petrology and geochemistry of shield picrites, Earth Planet. Sci. Lett, 168(1), 27- 44.

Ottonello, G., Moretti, R., Marini, L., Zuccolini, M.V., 2001. Oxidation state of iron in silicate glasses and melts: a thermochemical model, Chemical Geology, 174: 157-179.

Pearce, J.A., Bender, J.F., De Long, S.E., Kidd, W.S.F., Low, P.J., Güner, Y., Saroglu, F., Yilmaz, Y., Moorbath, S., Mitchell, J.G., 1990. Genesis of collision volcanism in Eastern Anatolia, Turkey. Journal of Volcanology and Geothermal Research 44, 189-229.

Pearce, J.A., Parkinson, I.J., 1993. Trace element models for mantle melting: application to volcanic arc petrogenesi, In: Prichard, H.M., Alabaster, T., Harris, N.B.W. Neary, C.R.e. (eds.) Magmatic Processes and Plate Tectonics, London: Geological Society of London Special Publication, 76, 373–403.

Petry, C., Chakraborty, S., Palme, H., 1997. Olivine-melt nickel-iron exchange Thermometer: cosmochemical significance and preliminary experimental results. Meteor Planet Sci 32:106-107.

Philpotts, A., Ague, J., 2009. Principles of igneous and metamorphic petrology, Cambridge University Press.

Putirka, K., Johnson, M., Kinzler, R., Longhi, J., Walker, D., 1996. Thermobarometry of mafic igneous rocks based on clinopyroxene-liquid equilibria, 0–30 kbar. Contributions to Mineralogy and Petrology 123(1): 92-108.

Putirka, K., 1999. Clinopyroxene + liquid equilibria to 100 kbar and 2450 K. Contributions to Mineralogy and Petrology 135: 151-163.

Putirka, K., Ryerson, F.J., Mikaelian, H., 2003. New igneous thermobarometers for mafic and evolvedlava compositions, based on clinopyroxene + liquid equilibria. Am Mineral 88:1542-1554.

Putirka, K., 2005b. Igneous thermometers and barometers based on plagioclase + liquid equilibriatestsofsome existing models and new calibrations. Am Mineral 90:336-346.

Putirka, K., Perfit, M., Ryerson, FJ., Jackson, MG., 2007. Ambient and excess mantle temperatures, olivine thermometry, and active vs. passive upwelling. Chem Geol 241:177-206.

Putirka, K., 2016. Amphibole thermometers and barometers for igneous systems and some implications for eruption mechanisms of felsic magmas at arc volcanoes. Am Mineral 101:851–858.

Richards, J.P., 2015. Tectonic, magmatic, and metallogenic evolution of the Tethyan orogen: From subduction to collision. Ore Geol. Rev. 70, 323–345.

Ridolfi, F., Renzulli, A., Puerini, M., 2010. Stability and chemical equilibrium of amphibole in calc-alkaline magmas: an overview, new thermbarometric formulations and application to subduction-related volcanoes. Contrib Mineral Petrol 160:45–66.

Ridolfi, F., Renzulli, A., 2012. Calcic amphiboles in calc-alkaline and alkaline magmas: thermobarometric and chemometric empirical equations valid up to 1,130 °C and 22 GPa. Contrib Mineral Petrol 163:877–895.

Righter, K., Leeman, WP., Hervig, RL., 2006. Partitioning of Ni, Co, and V between spinel-structuredoxidesand silicate melts; importance of spinel composition. Chem Geol 227:1-25.

Roeder, P. L., Emslie, R. F., 1970. Olivine– liquid equilibrium, Contributions to Mineralogy and Petrology **29**, 275 – 289.

Rollinson, H.R. (1993) Using geochemical data: evaluation, presentation, interpretation, Longman Group, UK lst edition, 352p.

Rotstien, Y., and Kafka, A.L., 1982. Seismiotectonics of the southern boundary of Anatolia, eastern Mediterranean regions, subduction collision and arc jumping, J., Geophys. Res., 87, 7694-7706.

Sayari, M., and Sharifi, M., 2014. SCG: A computer application for single clinopyroxene geothermobarometry. Italian Journal of Geosciences, 133(2), 315-322. http://www.doi.org/ 10.3301/IJG.2014.01.

Schmidt, M.W., 1992. Amphibole composition in tonalite as a function of pressure: an experimental calibration of the Al in hornblende barometer, Contributions to Mineralogy and Petrology, 110: 304-310.

Schweitzer, E.L., Papike, J.J., Bence, A.E., 1979. Statistical analysis of clinopyroxenes from deep-sea basalts, American Mineralogist, 64: 501-513.

Searle, M. P., Cox, J., 1999. Tectonic setting, origin and obduction of the Oman ophiolite. Geological Society of America Bulletin, 111: 104–122.

Shand, S.J., 1943. Eeuptive Rocks, John Wiley and Sons, NewYork.

Shengor, A., Kidd, W., 1979. Post-collisional tectonics of the Turkish-Iranian plateau and a comparison with Tibet. Tectonophysics 55, 361-376.

Shengor, A.M.C., Özeren, M.S., Keskin, M., Sakınç, M., Özbakır, A.D., Kayan, I., 2008. Eastern Turkish high plateau as a small Turkic-type orogen: Implications for post-collisional crust-forming processes in Turkic-type orogens. Earth-Science Reviews 90, 1-48.

Soesoo, A., 1997. A multivariate statistical analysis of clinopyroxene composition: empirical coordinates for the crystallization PT-estimations. Geological Society of Sweden (Geologiska Föreningen), 119: 55-60. http://www.doi.org/10.1080/11035899709546454.

Stampfli, G.M., Borel, G.D., 2002. A plate tectonic model for the Paleozoic and Mesozoic constrained by dynamic plate boundaries and restored synthetic oceanic isochrons. Earth Planet. Sci. Lett. 196, 17–33.

Sugawara, T., 2001. Ferric iron partitioning between plagioclase and silicate liquid: thermodynamicsand petrological applications. Contrib Mineral Petrol 141:659-686.

Sun, S.S., McDonough, W.F., 1989. Chemical and isotopic systematicsof oceanic basalts: implications for mantle compositions and processes, In: Saunders A.D. and Norry M.J. (Eds.), Magmatism in ocean basins, Geol.Soc. London. Spec. Pub, 42: 313-345.

Taylor, S.R., Mclennan, S.M., 1985. The continental crust: its composition and evolution- an examination of the geochemical record preserved in sedimentary rocks, Blackwell Scientific, Oxford , 312.

Tokel, S., 1985. Mechanism of crustal deformation and petrogenesis of the Neogene volcanics in East Anatolia, special publication of Turkey jeoloji kurumu, Ketin symposium, Eds. T. Ercan and Caglayan, M.A., 121-130.

Ustaömer, P.A., Ustaömer, T., Collins, A.S., Robertson, A.H., 2009. Cadomian (Ediacaran–Cambrian) arc magmatism in the Bitlis Massif, SE Turkey: magmatism along the developing northern margin of Gondwana. Tectonophysics 473, 99-112.

Vernon, R. H., Clarke, G. L., 2008. Principles of Metamorphic Petrology. Cambridge University Press.

Vynhal, C.R., McSween, H.Y., Speer, J.A., 1991. Hornblende chemistry in southern Appalachian granitoids: implications for aluminum hornblende thermobarometry and magmatic epidote stability, American Mineralogist, 76: 176-188.

Wells, P.A., 1977. Pyroxene thermometry in simple and complex systems .Contributions to Mineralogy and Petrology 62(2): 129-139.

 https://doi.org/10.5281/zenodo.16876847